Geochemistry of the (meta-)mafic rocks from the Gonzalito mining district, northern patagonia

Carmen I. Martínez Dopico, Kathryn A. Cutts, Mónica G. López de Luchi, Franco Pugliese

PII: S0895-9811(20)30433-8

DOI: https://doi.org/10.1016/j.jsames.2020.102890

Reference: SAMES 102890

To appear in: *Journal of South American Earth Sciences*

Received Date: 14 April 2020

Revised Date: 19 August 2020

Accepted Date: 7 September 2020

Geochemistry of the (meta-)mafic rocks from the Gonzalito Mining District, Northern Patagonia

Carmen I. Martínez Dopico[a*], Kathryn A. Cutts[b,c], Mónica G. López de Luchi[a], Franco Pugliese[d]

[a] *Instituto de Geocronología y Geología Isotópica, CONICET-Universidad de Buenos Aires, Av. Int.Güiraldes s/n Ciudad Universitaria, Buenos Aires, C1428, Argentina*
[b] *Applied Isotope Research Group, Departamento de Geologia, Escola de Minas, Universidade Federal de Ouro Preto, Morro do Cruzeiro, 35400-000, Ouro Preto, MG, Brazil*
[c] *Universidade do Estado do Rio de Janeiro, Rua São Francisco Xavier 524, Maracanã, Rio de Janeiro, 20550-900, Brazil*
[d] *Centro de Investigaciones en Ciencias de la Tierra (CICTERRA), CONICET- Universidad Nacional de Córdoba, Vélez Sársfield 1611, Córdoba, X5016GCA, Argentina.*

* corresponding author: Carmen Martínez Dopico, *email:* carmenmd@ingeis.uba.ar

Abstract

In spite of hosting one of the most important Pb-Ag-Zn mineralizations in Patagonia, the metamorphic history of the rocks of the Mina Gonzalito Complex (MGC; east of the North Patagonian Massif) is still unclear. The complex consists of schists, para- and ortho-derived gneisses, ranging from greenschist to amphibolite facies, and metamafic rocks. Leucogranites and pegmatites were intruded synkinematically. Field, petrological and thermochronological evidence indicates that the MGC experienced an early prograde path and metamorphic peak during the Early Ordovician (ca. 472 Ma), magmatism and localized post-peak deformation and re-equilibrium at lower pressure, followed by uplift during the Late Permian. The MGC is intruded by the calc-alkaline Santa Rosa Diorite (SiO_2 = 58.7-60.4 wt%; La_N/Yb_N = 7.2-10.5) and trachyte dike swarms in the Late Permian- Early Triassic. The mafic intrusives of the MGC form small schistose, massive and banded bodies interlayered within the gneisses and granites and recorded recrystallization of hornblende + plagioclase + quartz + titanite ± clinopyroxene ± biotite ± ilmenite. The metamafic rocks are mostly tholeiitic gabbros having SiO_2 (45.4-52.1 wt.%), TiO_2 (0.62-2.88 wt.%), flat REE patterns (La_N/Yb_N =0.48-2.76), although some pyroxene-banded varieties show higher ratios. Initial P–T modelling in the NCKFMASHTO system for the metamafic rocks defined P-T conditions between 550–730 °C and 1-4 kbar. Our data suggest that the protolith of the metamafic rocks was emplaced in a shallow environment, associated with underplating of mantle-derived magmas slightly modified by crustal contamination. The intrusion of mantle-derived magmas may have been related either to a magmatic arc or to a continental rift environment. The model involving an Ordovician intracontinental back-arc basin is favored herein because it can reasonably explain many other geological features of Early Paleozoic basement rocks from the northern Patagonia.

Keywords: Gabbros; Ordovician; North Patagonian Massif; Gondwana

1. Introduction

The assessment of the Early Paleozoic tectonic evolution of Patagonia is critical to building any model of the assembly of southwest Gondwana. Evidence of the pre-Mesozoic metamorphic history of the North Patagonian Massif, the northern block of Patagonia, has been sluggish and difficult to interpret mostly due to the poor exposures, inaccessibility of the outcrops and the lack of petrological studies to produce precise and reliable information for the main igneous and metamorphic events. This particularly applies to the Mina Gonzalito Complex -or Mina Gonzalito mining district (Aragón et al., 1999a; Giacosa, 1987, 1997; Ramos, 1975; Rosenman, 1972)- in which the protoliths of low and high-grade metamorphic rocks and syn-kinematic granitoids aged between 540 to 250 Ma are the main constituents of the Paleozoic "Northern Belt" of the North Patagonian Massif (Ramos, 2008) (Fig. 1). The Northern Belt (NB) was claimed to be the southern extension of either the Pampean/Famatinian/Gondwanides belts of the Sierras Pampeanas of Argentina (Rapalini et al. 2013; Pankhurst et al. 2006, 2014) (Fig. 1), or a continuation of the Ross-Delamerian Orogen of Antarctica (González et al. 2018). The NB manifests a protracted orogenic evolution from subduction related-arc-marginal basin and magmatism through crustal extension and metamorphism (540-470 Ma) (González et al. 2018; Pankhurst et al. 2014, 2006; Rapalini et al. 2013, 2010) coeval with bimodal intrusive magmatism (490-450 Ma) (Gozálvez, 2009; López de Luchi et al. 2014; Martínez Dopico et al. 2017a), followed by uplift and development of foreland basins (450-360 Ma) (Rustán et al. 2013; Uriz et al. 2011) and widespread intracontinental magmatism in the context of a Permo-Triassic Large Igneous Province (280-240 Ma) (Luppo et al. 2018; Martínez Dopico et al. 2019; Rapela and Caminos 1987) (Fig. 1).

The Early Cambrian -Ordovician metasedimentary and igneous basement rocks of the North Patagonian Massif outcrop as variably deformed discontinuous, sequences trending roughly NE-SW and NW-SE that are separated by Paleozoic km-scale shear zones and intruded or covered by Late Permian to Early Triassic plutonic-volcanic igneous complexes. The basement comprises the Cambrian Tardugno orthogneiss (529 ± 4 Ma and 522 ± 4 Ma; U-Pb SHRIMP zircons, Rapalini et al. 2013, Pankhurst et al. 2014) and three metamorphic sequences with lithological and geochronological similarities: 1) phyllites, schists, metagreywackes, and intercalations of mafic and acidic igneous rocks that crop out close to Nahuel Niyeu, Valcheta and Aguada Cecilio localities (Nahuel Niyeu Formation; Chernicoff, 1994; Chernicoff and Caminos, 1996; Greco et al. 2015, 2017; Martínez Dopico et al. 2014); 2) greenschist facies slates, phyllites, metaigneous schists, and metaconglomerates of the El Jagüelito Formation (González et al. 2018) that outcrop along the Salado river; and 3) the medium to high-grade para- and ortho-derived schists, gneisses, amphibolites, and granites of the Mina Gonzalito Complex (MGC; Giacosa 1987). The age of metamorphism of the MGC was estimated at ca 472 Ma (Greco et al., 2014; Pankhurst et al. 2006) based on metamorphic rims of zircons from para-derived gneisses of the MGC. This metamorphic age has turned out to be problematic due to the undeformed subvolcanic granitic and tonalitic intrusions, dated at 476 ± 6 Ma (U-Pb SHRIMP zircon ages; Pankhurst et al., 2006). These intrusive rocks not only contain metamorphic enclaves of phyllites, schists and mafic rocks, but they also crosscut the slates and phyllites of the El Jagüelito Formation. This sort of geological evidence is also recorded in the >470 Ma Valcheta Pluton that is hosted by the low to medium-grade metaclastic rocks of Nahuel Niyeu Formation (López de Luchi et al., 2008; Gozálvez 2009).

This study aims to constrain the nature of the “high-grade” metamorphic basement of the Mina Gonzalito Complex (Giacosa, 1987, 1997; Pankhurst et al. 2001) (Fig.1) and to discuss the origin of the protoliths of its metamafic rocks and the tectonic setting in which they were formed, based on the integration of stratigraphic, petrographic, WR-geochemical analyses and preliminary thermodynamic modelling using *Theriak/Domino* (De Capitani and Petrakakis, 2010). The ultimate goals are to understand the connection of the Mina Gonzalito Complex to the other metamorphic sequences and to clarify their geodynamic significance in the context of the assembly of southwest Gondwana in the Early Paleozoic.

2. Geological overview of the Mina Gonzalito area

The Mina Gonzalito mining district (Ramos 1975; Aragón et al. 1999a) is an igneous-metamorphic block that hosts the most important polymetallic deposit (Pb-Ag-Zn, Cu-V, fluorite and In ore) in northeastern Patagonia (Aragón et al. 1999a; Del Mónaco 1971; Pugliese et al. 2019; Vallés 1978 and references therein). It is located to the southeast of the Sierra de Pailemán, 100 km to the southwest of San Antonio Oeste, in the Río Negro province of Argentina. The block is limited to the west by the Jagüelito shear zone, which separates the MGC from the low-grade metamorphic rocks of the El Jagüelito Formation (Giacosa, 1987) and Ordovician muscovite and garnet-bearing leucogranites (471 ± 2 Ma U-Pb SHRIMP zircon dating; Peñas Blancas Granite, García et al. 2012). Its northern boundary is marked by the Arroyo Tembrao creek where metamorphic rocks are crosscut by mid-Permian biotite-bearing tonalitic and granodioritic orthogneisses and leucogranite dykes (ca. 265 Ma- Arroyo Pailemán and Tembrao plutons; Grecco et al. 1994; Tohver et al. 2008) and pierced by the Jurassic eruptive centre of the Sierra de Paileman (188 ± 1 Ma; Marifil Complex;

Cortés 1981; Pankhurst et al. 2000). To the south and southeast, the block is covered by a NE-SW fringe of alluvial deposits. Our study area is limited to the rocks located between the south of the Sierra de Pailemán, the east of the El Jagüelito shear zone and Estancia Santa Rosa locality (Fig. 2).

The rocks from the Mina Gonzalito mining district were collectively known under the name of Mina Gonzalito Complex (Busteros et al. 1998; Giacosa 1987, 1997) and distinguished from the Early Triassic trachyte dykes and lava flows (243.6 ± 1.7 Ma, U-Pb LA-ICPMS in zircon age; González et al. 2014) and several Early Jurassic rhyolitic dyke swarms that intrude them.

In the area of study (Fig. 2) the MGC comprises:

i) Fine to medium-grained banded biotite and biotite-muscovite bearing schists and gneisses (e.g. Mina Gonzalito Gneiss of Ramos, 1975; Fig. 3a,b) intruded by ii) variably deformed (muscovite or muscovite/garnet) leucogranites and aplitic and pegmatitic dykes (Giacosa 1987; Busteros et al. 1998); Available U-Pb zircon SHRIMP ages for a biotite-garnet paragneiss from two different localities indicate the same age, ca 472 Ma, which was interpreted as the age of the metamorphic peak (Pankhurst et al. 2006; Greco et al. 2014).

ii) María Teresa and Tapera plutons (Ramos 1975), that were emplaced as stocks and sills and syn-kinematically deformed with the host; The former is a small porphyroclastic leucogranitic stock (<10 km^2) that is mostly composed of quartz + K-feldspar+ plagioclase + muscovite + garnet, whereas Tapera pluton is larger (>15 km^2) and, according to Giacosa (1997), it is a muscovite bearing granite that contains a variable amount of biotite. Grecco and Gregori (2011) dated muscovite and biotite grains from rocks considered part of María Teresa and Tapera plutons that yielded Ar-Ar mica-plateau ages of 261 ± 2 Ma and 264 ± 2 Ma, respectively.

iii) Partially retrogressed (meta)mafic rocks and amphibolitic schists that occur in lenses and layers within the banded biotite gneiss or isolated (not showing contacts) (Fig. 3c). Part of these rocks were called “black schists” by Aragón et al. (1999a).

iv) Occurring in the west of the block are medium- to coarse-grained, mostly weakly foliated, biotite-bearing orthogneisses (Varela et al. 2011) and quartz-diorites that intrude (i) the gneisses; Varela et al. (2011) dated a granodioritic orthogneiss that yielded a U-Pb zircon SHRIMP age of 492 ± 6 Ma.

v) Marbles and siliciclastic levels were described by Giacosa (1997) and Dalla Salda et al. (2003) to the south of Estancia Santa Rosa along the Salado creek.

Within the block, the structural style and lithological features change from east to west defining two different zones that are separated by an NNW-SSE ductile shear zone. González et al. (2008b) indicated that towards the west, the MGC is dominated by the medium grade, largely injected paragneisses and intermediate to acidic synkinematic granites and pegmatite dykes. Orthogneisses are frequent in this area. In contrast, to the east, the magmatism and presence of “amphibolite” lenses become negligible and the para-derived rock would have achieved lower metamorphic conditions. Giacosa (1997) considers that the maximum peak metamorphic conditions reached the transition between greenschist and amphibolite facies. On the other hand, Aragón et al. (1999a) indicates that the sillimanite-garnet-plagioclase bearing leucogranites could have an anatectic origin. Most rocks of MGC were widely deformed, fractured and infilled with quartz-Pb-Zn-Ag ore-rich infilling in veins and fractures during the Early Jurassic (Pugliese et al. submitted).

3. Field relations and sample description

The rocks of the Mina Gonzalito Complex are very poorly exposed with exception of the mine shafts opened during the mining works 50 years ago. The most striking landforms exposed across the block are NNW-SSE leucogranite ridges (aplites and pegmatites) that stand out in the landscape due to differential weathering of the gneisses, schists and small (meta)mafic bodies (Fig. 2). The ridges are roughly parallel to strike of the Early Triassic trachyte dykes (243.6 ± 1.7 Ma; González et al. 2014). To ease the description, and following González et al. (2008b), we are going to divide the crustal block using the WSW-ENE road to Los

Berros into western (including the Tres Marías and María Teresa mines, and Puesto Dragón exposures), central and eastern (from Puesto El Panchito to Gonzalito mine) sectors (Fig. 2). For this study we sampled the biotite gneisses, granites, (meta)mafic rocks and diorites. The lithologies will be described first and then the samples used for thermodynamic modelling.

3.1. Biotite gneisses and schists

The most common unit among the pre- Triassic rocks of the study area comprises grey to brownish biotite bearing schists and gneisses, interlayered with (meta-)mafic lenses or schollen, that are variably injected and intruded by leucogranitic material at the scale of centimeters to tens of decimeters that sometimes forms individual stocks (Fig. 3a, b). Para-derived rocks dominate to the east, while synkinematic leucogranites and granitic orthogneisses are more frequent to the west.

Brown to grey schists and gneisses are generally fine to medium-grained, layered or banded, mesocratic metamorphic rocks of mostly tonalitic composition that are characterized by their lepidoblastic to granolepidoblastic texture (Fig. 3a, b) and a very variable degree of leucocratic injection. From the mineralogical point of view, the schists are composed of quartz, biotite, plagioclase and, occasionally, late muscovite. At a macroscopic scale, wherever their grain-size is coarser, they are banded with brownish-grey and white layers. The banding is folded. The white bands are coarser-grained and poor in mafic minerals whereas the darker bands contain principally biotite. Some of the leucocratic sheets appear as if they have been intruded after the formation of the banding, as they cut across it. Their most common mineral assemblage of the gneisses contains biotite, quartz, plagioclase, sometimes muscovite and minor garnet (Fig. 3b; 4a-d). Common accessory phases in the matrix are apatite, zircon, opaque minerals and magnetite. Biotite and quartz are the most dominant minerals together with plagioclase.

Gneisses and schists (i.e. around Mina Gonzalito mine camp) contain euhedral to subhedral flakes of red-orange or reddish-brown to light yellow biotite (Fig. 4a-b); whenever the content of the mineral is higher, the S1/2 fabrics are strongly developed and become a gneissose fabric (layering < 2-3 cm) with leucocratic bands composed of quartz, plagioclase and muscovite. Biotite is occasionally retrogressed to chlorite and opaque minerals. Quartz has some polygonal shapes resembling a recrystallized matrix whereas plagioclase remains subhedral in shape. Some plagioclase crystals show complete polysynthetic twinning and no zoning, but most of them are not twinnedTo the southeast of the block, the rocks acquire a light-grey bluish colour and porphyroclastic texture with sigmoid-shaped plagioclase porphyroclasts within a fine-grained recrystallized mylonitic biotite-quartzitic matrix. The alteration is variable, and mostly to sericite and clays along fractures and cleavage planes. There is a significant variation in the grain size of plagioclase, indicating that these crystals could have been part of the phenocryst and matrix phases of the protolith. The muscovite/biotite ratio is low. Muscovite is anhedral, frequently found with biotite but also often isolated, occasionally surrounding small chips of subhedral garnet. Within the schists, garnet is infrequent, anhedral and colourless, and, where it occurs, it makes up less than the 2% of the rock (Fig.4a). Two episodes of blastesis of muscovite can be detected in the gneisses: fine-grained crystals associated with biotite and larger crystals that are incongruent with the fabric of the rocks, which developed with symplectites and quartz. Garnet has been observed in some sampling sites. Larger crystals are mostly found in leucocratic injections within the gneiss where red garnet crystals up to 4 cm in diameter appear within the leucocratic bands, suggesting that might be a peritectic product of partial melting. The occurrence of sillimanite and cordierite has been reported by Aragón et al. (1998) and González et al. (2008b). Sillimanite was only observed in some thin sections of the leucogranites, formed at expense of with muscovite.

3.2. Metamafic rocks

Both brown to grey and bluish-grey gneisses of the Mina Gonzalito enclose scattered concordant lenses or layers of dark green mafic rocks that vary from tens of meters to just a few meters in length. These rocks have broad textural and compositional variation. Aragón et al. (1999) interpreted these as mafic dykes or sills emplaced before or during regional metamorphism and referred to some of these rocks as “black schists” whenever they were fine-grained and altered to chlorite + carbonates. The basic rocks encompass different types of massive to variably deformed hornblende ± biotite, and hornblende, and diopside-hornblende banded (meta)igneous rocks and, more rarely, hornblende schists. These rocks tend to be darker when the schistosity is defined by amphibole rather than by biotite parallel orientation, constituting fine-grained nematoblastic to granoblastic textures (Fig 5a-b). The grain size is quite variable, from medium (2-3 mm) to fine-grained (<1 mm). They are mostly massive or slightly foliated (Fig. 5c) and more rarely banded and folded (Fig. 5d) such as in the Tres Marías and Polito mineshafts, in the western and eastern sectors of the block, respectively. The massive metamafic rocks are transitional fine to coarse banded types such as in Tres Marías Mine (Fig. 5 c-d).

Most of the metaigneous rocks are gabbros (or hornblendites) and microgabbros that show polygonal granoblastic texture and their mineral composition is dominated by zoned reddish-brown to brown (>60 % modal Fig. 5a, c; Fig. 6b) or bluish-green to green and green hornblende (Fig. 5c,d; Fig. 6c) and subhedral zoned and polysynthetic-twinned plagioclase (25-20%; mainly Andesine-Labradorite). Minor biotite is present. Titanite, ilmenite, quartz, and apatite are accessory minerals. Quartz crystals seldom appear in the mosaic interstices. In some rocks, amphibole, plagioclase and quartz recrystallization is evidenced with triple point junctions, whereas others maintain igneous textures. In addition, close to the faults these rocks are highly strained and sometimes retrogressed or altered.

Wherever the metamafic rock with bluish green to green and green hornblende bearing rock is banded, biotite disappears, and light green to colourless clinopyroxene (diopside) and highly coloured hornblende occurs. The diopside and hornblende are concentrated in layers from one to ten millimetres thick that define the compositional banding (Fig.4a, f). The banded types also contain plagioclase, titanite, and minor amounts of quartz, and apatite. The compositional banding seems to be an inherited condition from the protolith since it grades to a non-banded amphibolite. This banding has also been observed to be folded near Gonzalito mine. In this area, certain banded metamafic rocks are spatially associated with diorites. The metamafic rocks studied in this work show no evidence of melting, such as patches of neosome or any of the peritectic phases expected after fluid-absent melting reactions in this type of hornblende-bearing rock.

Some of the schists interlayered in the gneisses are lighter than the hornblende-bearing metamafic rocks. They show lepidoblastic toporphyroblastic textures with coarser crystals of zoned plagioclase immersed in a matrix that contains reddish-brown to yellow biotite, quartz, titanite and seldom hornblende, although some of them are partially to totally retrogressed to a light green clinoamphibole, epidote, sericite and opaque minerals. These rocks were not sampled for geochemical analyses.

These metamafic rocks have a variety of mineral assemblages and textures which are described in detail for the modelled samples below.

Sample 31/32-3

This sample is from the Las Tres Marias mineshaft in the northwest of the study region (Fig. 2) and contains clinopyroxene, amphibole, titanite, ilmenite, plagioclase and quartz (Fig. 4a). The rock is banded with discrete domains dominated by light green clinopyroxene (up to 300 μm) and the reminder of the rock is dominated by amphibole (up to 500 μm in size). The amphibole is highly coloured from the dark green to light brown. Along with the banding, the rock preserves a foliation that is defined by elongate clinopyroxene grains and amphibole grains. Both ilmenite and titanite are present in the rock, although titanite is more common. Ilmenite usually occurs on the rims of titanite. Titanite is also observed as an inclusion in amphibole.

Plagioclase and quartz are equidimensional to elongate (up to 200 µm, parallel to the foliation) and polygonal (Fig. 6a).

Sample P8-2B

Sample P8-2B is from the Gonzalito mineshaft in the eastern sector of the study region (Fig. 2) is an amphibolite with lighter bands (S0/S1) mostly composed of clinopyroxene and plagioclase and darker bands with a predominance of clinoamphibole. It contains light green clinopyroxene, green to light brown amphibole, titanite, ilmenite, plagioclase, quartz and apatite. Titanite occurs throughout the sample as fine grains. Ilmenite occurs as large discrete grains.

Sample 20-4

This sample was obtained close to the Gonzalito mine camp in the eastern sector of the study region (Fig. 2) and contains the minerals amphibole, plagioclase, ilmenite, biotite and quartz. In the field, the rock constitutes massive levels with a coarse-grained texture (with plagioclase and amphibole grains up to 1 mm in size; Fig. 6b) within a gneissic host. It has a granoblastic texture mostly composed of euhedral brown to light-orange brown clinoamphibole (>50%). This clinoamphibole is recrystallized from another clinoamphibole. Biotite is rare, where it occurs it is subhedral and commonly replaced by chlorite. Ilmenite is fine-grained (< 100µm) and occurs as inclusions in amphibole and on amphibole grain boundaries (Fig. 4c). Plagioclase (~An_{45-55}) is subhedral, zoned and it is sericitized on grain edges and cracks within the grain.

Sample 22-3

This sample comes from the Puesto El Panchito in the central region of the study area (Fig 2). It contains the minerals clinoamphibole (>50%), plagioclase, titanite, ilmenite and quartz. The sample is massive and granoblastic (grains are usually 300 µm but amphibole can be up to 500 µm) with a very weak foliation defined by the preferred orientation of the clinoamphibole grains (Fig. 6c). The clinoamphibole is mostly euhedral and shows green to light-yellow pleochroism and has zircon inclusions. Plagioclase is subhedral and most of the crystals are devoid of twinning. The amount of quartz is below 5%. The ilmenite is finer-grained (<100 µm) and occurs in the matrix or as inclusions in amphibole. Titanite occurs as small clusters of grains and also as cores to some ilmenite grains.

3.3. Granites

Several types of injections, i.e. acidic aplites, granites and pegmatites, in the gneisses and schists occurred in Mina Gonzalito block. In general, the volume of leucocratic material increases towards the west, and close to El Jagüelito shear zone where leucogranites are either injected into the host or form sills and plutons emplaced mostly in sigmoid structures along a N20-30°W fringe (Fig. 2). There are two main leucogranite bodies: the María Teresa stock (muscovite bearing type) and the Tapera laccolith (a garnet-mica-bearing pink leucogranite), intruded parallel to the S1 or S2-fabric of the host. Most of them are boudinaged, medium to coarse-grained differentiates or aplitic dykes and sills of leucogranitic composition. These are mostly concordant with the schistosity and seem to have been synkinematically emplaced, resembling leucocratic schists. The dominant paragenesis is Qtz + Kfs + Pl + Ms (Sill) ± Grt and their foliation can be seen by sight through the alignment of muscovite flakes. These rocks have a fine to medium-grained equigranular texture where quartz and feldspars are the most abundant minerals. Muscovite, the main accessory mineral, often forms fibrous aggregates (nests) that develop into sillimanite -fibrolite when in contact with quartz. The appearance of sillimanite suggests that they have been metamorphosed with the hosting gneiss. Garnet crystals are pink with euhedral shapes and typically undeformed. Towards the borders of the synkinematic leucogranitic intrusions (i.e. P20), the amount of biotite and plagioclase increases (biotite-bearing facies)

Aplopegmatite bodies crosscut the sequence. In the easternmost sector, leucocratic veins that inject the biotite-quartz bearing-gneisses are composed mostly of perthitic microcline and quartz, and minor plagioclase and fine-grained muscovite, which is reacting to sillimanite towards the border of the aggregates. Injection is limited around Tres Marías mine. But, to the south, in the surroundings of Puesto Dragón, where the synkinematic Tapera Pluton outcrops, the leucocratic bands in the host increase in grain size and abundance at the expense of the biotite-rich melanosome. In this area, the granite transitionally acquires a higher amount of biotite. This transitional rock could be that described by González et al. (2008) as a granodioritic orthogneiss, and later on as a tonalitic orthogneiss by Varela et al. (2011).

To the east, leucocratic injections are also synkinematic with the S2-fabric of the gneiss although they occur less frequently than to the west. In the central sector, they are resolved as NNW-SSE leucogranite sills and dykes composed of microcline, quartz, muscovite (sillimanite) and scarce brown to pale yellow biotite flakes (colour index <5%). This suggests that the leucogranite injection could be related to the synkinematic muscovite ± garnet-bearing intrusions. There are also aplite leucocratic veins that crosscut the folded metamafic rocks and biotite bearing schists.

Interestingly, in the eastern and central sectors of the block the structural grain is given by the S2 gneissose fabric and/or schistosity of the metamorphic protolith which is N10º to 50ºW dipping to the NE. Around the Tapera pluton, the foliation pattern is more complex and shows a SW-NE strike.

3.4. Santa Rosa Diorite

This unit, first described here, crops out close to the locality Estancia Santa Rosa. It is made up of a stock of dark green to brown medium-grained diorite that intrudes the brownish-grey gneisses. The limits of the stock are unknown due to the poor-exposures. The rocks display an unevenly-granular hipidiomorphic texture and contains spongy-looking brown to green to light green hornblende crystals (30%) in a matrix of plagioclase (20-25%), dark brown to yellow biotite flakes (25-20%), quartz (15%) and a few crystals of titanite (2%), magnetite, apatite, and zircon (<4%). The hornblende crystals are typically subhedral to euhedral and free of alteration. They form either larger crystals with corroded cores or clots composed of aggregates of smaller crystals surrounded by biotite, both of similar size.

Corroded pyroxene and/or clinoamphibole cores are commonly found within hornblende crystals. Polysynthetic twinned plagioclase (andesine) is subhedral. Apatite also can occur as larger crystals. Notably, opaque minerals are surrounded by a titanite rim. Alteration is infrequent but restricted to chlorite and opaque minerals.

Although most of the stock is massive, locally, rocks dramatically change their grain size by shearing and recrystallization. There, the grain size is finer and the amphibole crystals are strongly aligned.

Even though these rocks were only identified as a coherent body around Estancia Rosa, diorites were found around Mina Gonzalito mineshaft (site P8). These diorites are fine-grained equigranular and contain mostly brownish-red to yellow biotite, light green to yellow hornblende, zoned plagioclase, quartz, titanite and apatite. However, they do not show evidence of recrystallization.

4. Methods

4.1. Whole-rock geochemical analyses

Samples were collected by Dr L.H. Dalla Salda and coworkers in two field trips to Gonzalito mining district during the middle 90`s (Table 1), mostly at old abandoned shafts of the Gonzalito, María Teresa and Tres Marías mine camps. Major and selected trace and rare earth element (REE) determinations were performed on samples up to 2-3 kgs and screened based on the thin sections. Twenty-five samples of metamafic rocks, gneisses and granites in the Mina Gonzalito Complex and Santa Rosa Diorite were determined using X-ray fluorescence spectrometry (XRF) and inductively coupled plasma mass spectrometry

(ICP-MS) at Activation Laboratories Ltd., Ontario, Canada. The results are presented in Table 1 separated by lithology and, in the case of the low-silica rocks, distinguishing the association of biotite-hornblende, hornblende, or hornblende-pyroxene. Part of the geochemical results were presented in Aragón et al. (1999a, b). In the text and figures, all compositions are recalculated to 100% anhydrous to minimize the effect of alteration on the samples.

Alkali-elements show some scatter and probably were slightly modified by secondary processes in some samples, particularly those sampling sites located close the hydrothermal epicentre such as Gonzalito, Vicentito, Polito, Tres Marías and María Teresa mines (Aragón et al. 1999). Samples that yield relatively high LOI values (>4%), reflecting rock alteration, were excluded (i.e., GoPi-3; GoPi-4). The effect of weathering and alteration was further evaluated with the FMW parameters proposed by Ohta and Arai (2007) (Supplementary appendix A) and this allowed us to exclude samples P4-3 and P3-4 6a. The dataset was compared to that of the amphibolites and granites of Tapera and María Teresa plutons of Busteros et al. (1998) and Giacosa (1997), and the metaperidotite and gabbro sill within the Nahuel Niyeu Formation of Greco et al. (2015). The relations and ratios between the elements were analysed with the GCDKit 6.0 software (Janousek et al. 2006) and the scripts in Janousek et al. (2015).

4.2. Pressure-temperature calculations

Four P–T pseudosections were calculated for the metabasic rocks: two samples of the banded pyroxene-bearing rock from the Gonzalito shaft (sample P8-2B) and Las Tres Marías mine (P31/32-3), and two massive metamafic rocks (samples 20-4 and 22-3) from the Vicentito mineshaft and surroundings of Puesto El Panchito, respectively (Fig. 2). Pressure-temperature pseudosections were calculated using the software package Theriak/Domino (De Capitani and Petrakakis 2010) and the updated database of Holland and Powell (2011). The geologically realistic system NCKFMASHTO (Na_2O-CaO-K_2O-FeO-MgO-Al_2O_3-SiO_2-H_2O-TiO_2-Fe_2O_3) was used for all samples. The bulk composition of all samples was determined by whole-rock XRF analysis. Our study lacks EPMA mineral composition data to support our results, therefore they should be considered as strictly preliminary.

For all samples, the mineral assemblages and field observations indicate P-T conditions to be subsolidus. For this reason, H_2O was set in excess. The proportion of Fe_2O_3 to FeO has been estimated by considering the abundance of Fe^{3+} bearing minerals and modal constraints in the context of recalculated EDS analyses -using the methods of Droop (1987) and Tindle and Webb (1994)-. A T-$M$$Fe_2O_3$ or P-$M$$Fe_2O_3$ diagram was then calculated to determine if these estimates were appropriate. The percentage of total iron set as Fe^{3+} for samples 31/32, P8-2B, 20-4, and 22-3 was 20%, 30%, 10 and 0-10%, respectively. The 'metabasite set' of models from Green et al. (2016), converted to Theriak-Domino format by Doug Tinkham (see Jorgensen et al. 2019) were applied for samples 31/32, P8-2B, 20-4, and 22-3. These are White et al. (2014) for orthopyroxene, garnet, biotite, muscovite and chlorite; Green et al. (2016) for clinoamphibole, augite and metabasite melt; Holland and Powell (2011) for olivine and epidote; Holland and Powell (2003) for plagioclase; White et al. (2002) for spinel and magnetite and White et al. (2000) for ilmenite.

5. Results

5.1. Geochemical characteristics

The rocks of Mina Gonzalito Complex and Santa Rosa Diorite show a discontinuous range of silica on the TAS (total alkali-silica; Cox et al. 1979) diagram, where they plot from gabbroic and dioritic to granitic rock compositions, respectively (Fig. 8a). In the AFM diagram (Fig. 8b; Irving and Baragar 1971) the amphibolites and hornblende schists follow a tholeiitic trend. In contrast, the Santa Rosa diorites, together with the gneisses and leucogranites of the Mina Gonzalito Complex, show high SiO_2 values corresponding to the calc-alkaline trends, as expected. A more precise classification is attempted based on high field strength elements (HFSE), which are less sensitive to metamorphic mobility. Accordingly, the low Nb/Y ratios (< 0.7) for most of the samples indicate a clear subalkaline tholeiitic affinity (Winchester and Floyd, 1977) Fig. 8c). Two samples from a banded amphibolite have higher Nb/Y values suggesting an alkaline character, however, since the rocks underwent at least one metamorphic event and, as will be discussed below, substantial evidence would support that these two samples could represent cumulate rocks; therefore their alkaline character, among other geochemical features, should be regarded with caution.

The binary diagrams of major and highly compatible elements using MgO as a variation index are shown in Figure 9. The arrangement of the sample set is a discontinuous semi-linear layout that reflects the different nature of the protoliths and a wide variation within the metamafic rocks.

5.1.1. Metamafic rocks

The major elements of the metamafic rocks of the Mina Gonzalito Complex -amphibolites - show a basic composition, with low to moderate SiO_2 (45.5-52.2 wt.%) and Al_2O_3 (12.5-16.1 wt.%) and moderate to high contents of MgO (5.8-9.5 wt.%) and Fe_2O_3t (9.6-17.4 wt.%). Although there is a wide dispersion in CaO contents (9.2-17.4 wt.%) in comparison with MORB-type reference values (Gale et al. 2013) (Fig. 9), the rocks with values > 14 wt% are those that are banded. Their Mg number (Mg# = 100 * molar MgO/ [MgO +FeO_t]), an index of fractionation in basaltic liquids, are between 47 and 69. The average total alkali content (Na_2O + K_2O) is around 2.1 wt. % (only one sample exceeds 3%), which is lower than the MORB average values. Conversely, most of the hornblende-bearing amphibolites have TiO_2 contents lower than 2 wt. %, similar to the MORB reference values (Gale et al. 2013).

The rocks exhibit high Cr/Th (>50) and low Th/La (<0.15), together with low Zr/Ti ratios (<0.02) with low Ni contents (<250 ppm) (Fig. 4b), suggesting a basic magmatic precursor rather than a sedimentary protolith. All the hornblende ± biotite- bearing amphibolite and schists exhibit a similar trace element pattern and low REE total content. Most of them show low Zr/Y (<4.5), Ti/Y (<350) and La/Nb (<2) ratios, similar to the MORB reference values.

Chondrite-normalized rare earth element (REE) spidergram (Boynton 1984) of the metabasites and schists show a gently sloping to flat pattern, commonly with $(La/Yb)_N$ ratios between 0.5 and 2.8, $(Eu/Yb)_N$ ratios between 0.8 and 1.2, and weakly negative to positive inferred Eu anomalies ($Eu_{CN}/((Sm_{CN}*Tb_{CN})*0.5)$ =0.74–1.14) (Figs. 10,11). Indeed, REE concentrations are between only 10 to 20 times higher than the chondritic values. Therefore, the flat REE patterns would appear to preclude significant crustal contamination of the parental magmas of these amphibolites. Two samples of the clinopyroxene-bearing amphibolites exhibit a higher REE content (>200), steeper slope in chondrite-normalized REE plot (La/Yb>10), and TiO_2 contents over 2 wt.%, suggesting that they may be cumulates (perhaps with a higher proportion of clinopyroxene and ilmenite?) in the ancient protolith.

In N-MORB and Primitive Mantle (Sun and McDonough 1989) normalized multielement spidergrams, the selective enrichment in some LILE (Large Ion Lithophile Elements such as Cs, Rb, Ba, and Th, and Pb - although the latter is here mostly related to the hydrothermal fluid alteration) and, to a lesser extent, in light REE (La, Ce, and Nd) and depletion in fluid-immobile HFSE (High-field strength elements; Nb, Zr, Eu, Hf, and Tb) (Fig. 11a and b) are observed. However, the enrichment in LREE relative to HREE is up to four times the N-MORB and only slightly poorer than the E-MORB reference values of Sun and McDonough (1989) and Gale et al. (2013). The pyroxene-bearing metabasites are enriched between three to four times relative to the E-MORB, but their chemistry would not represent those of melts. Moreover, the patterns of immobile elements relative to the N-MORB show negative Nb anomalies characteristic of phase-fractionation in subduction-related magmas (Saunders and Tarney 1979).

5.1.2. Gneisses and leucogranites

Silica values vary between 69.05 and 70.9 wt. % in the gneisses, whereas in the gneiss-hosted leucogranites (leucosomes?) contents are higher than 73 wt. %. Similarly, compositions of the former are “granodiorites” (4.7 <K_2O+Na_2O< 6.0 wt.%), whereas the latter are “granites” (5.9 <K_2O+Na_2O< 7.9 wt.%) in the TAS diagram (Cox et al., 1979). They are characterized by high contents of Fe_2O_3t+MgO (7.08-8.28 wt.%) and low TiO_2 (0.7-0.9 wt.%). The gneisses are strongly peraluminous with ASI values ranging from 1.27 to 1.39.

Leucogranites are peraluminous with alumina saturation indices ASI and A/CNK (molecular Al_2O_3/CaO+Na_2O +K_2O, with or without CaO corrected for apatite) between 1.21 and 1.39 (typical A/CNK values for S-type granite are 1.10-1.30; Chappell and White (2001)), low CaO (0.67-1.18 wt.%) and high K_2O (3.87-5.11 wt.%) concentrations with strong variations in Na_2O and CaO. Total Fe_2O_3 + MgO is <5%. These concordant leucogranites have K (atomic calculated at 100% anhydrous base) between 0.08 and 0.09 and Ca/(Ca + Na) between 0.11 and 0.24, Fe+Mg between 0.02 and 0.07 contents, similar to those of experimental S-type melt compositions generated between 775 and 900ºC from the melting of metasedimentary starting materials (compilation in Taylor et al. 2014).

The gneisses have a roughly steep REE pattern with (La/Yb)N ratios ranging from 6.2 to 10.7, (Eu/Yb)N ratios between 1.1 and 1.5, and negative inferred Eu anomalies (EuCN/((SmCN*TbCN)^0.5) =0.50–0.71). In contrast to the gneisses, leucogranites have lower total REE (>170 and >156 ppm, respectively). In the MORB-normalized trace element plots (Fig. 9) all the gneisses exhibit significant enrichment in LIL elements, e.g. Cs, K, Rb, Ba, Pb, but relative depletion in Sr and high field strength elements (HFSEs, Nb, Ta, Ti) and P.

5.1.3. Santa Rosa diorites

The Santa Rosa intrusion is composed of mostly undeformed magnesian calk-alkalic diorites (Fig.7a-c). In comparison to the amphibolites and amphibolitic schists of Mina Gonzalito Complex, they are richer in SiO_2 (58.7-60.3 wt.%) and poorer in Fe_2O_3t (7.9-8.6 wt.%), MgO (4.3- 4.9 wt.%) and CaO (4.6-5.8 wt.%). Alumina contents are around 15 wt.%. The diorites are metaluminous with ASI values in the range of 0.87 and 0.99 and phosphorous content between 0.34 and 0.41 wt.%. The Na_2O/K_2O ratio shows little variation, from 0.85 to 1.1, but their high potassium content, together with the high Th (9-11 ppm) and Co (21-25 ppm) contents, allow these rocks to be classified as shoshonitic to high K-calc-alkaline according to Hastie et al. (2007) and Peccerillo and Taylor (1976).

The Santa Rosa diorites have a higher REE content (>150 ppm) and very different patterns on a chondrite and N-MORB-normalized diagrams in comparison with other rocks of the complex (Table 1). Typically they are moderately enriched in LREE ([La/Yb]N=7.25–10.5, Fig. 5) and show concave-like middle to heavy REE pattern ([Eu/Yb]N =1.7-2.0; Table 1).

5.2 P-T modelling

We used the whole-rock XRF bulk composition of four samples to assess their equilibrium conditions using Theriak-Domino. The results obtained herein should be considered as strictly preliminary since our study lacks a reflective microscopy study and EPMA mineral composition data to study potential missing mineral phases (i.e. inclusions) and mineral zoning (i.e. amphibole; plagioclase).

- Sample 31/32-3 (Las Tres Marías mineshaft; northwest) has an interpreted mineral assemblage of clinopyroxene + amphibole + titanite + ilmenite + plagioclase + quartz. Using an Fe^{3+} content of 20%, this field occurs on the diagram at 650-730 °C and 1-3 kbars (Fig. 12b). This field is limited by the solidus up temperature and the stability of ilmenite and titanite (both are observed in the sample). If the Fe^{3+} content is varied (reduced to 10% Fe^{3+}; Supplementary material B; figures C,D), then this stability field occurs at 3-4 kbar and 680-730 ºC and is limited by the loss of quartz at low P, and ilmenite and titanite at low temperature and high temperature respectively (Supplementary material B, figures C, D). If the amount of Fe^{3+} is increased, quartz stability increases down pressure but the position of the peak field in terms of temperature does not change. The modelling for this sample indicates the presence of biotite, which was not observed in the sample. The calculated mode of biotite is quite low (<5%) and potentially its inclusion is a result of including potassium in the modelling.

- Sample P8-2B (Gonzalito mineshaft; eastern sector of the block) contains clinopyroxene + amphibole + titanite + ilmenite + plagioclase + quartz + apatite. Since apatite cannot be modelled, the total amount of CaO was reduced by approximately 4 wt.% corresponding to the 2-3 % apatite observed within the rock. A *T-M*CaO diagram was calculated to evaluate the effect of removing the apatite (see supplementary material figure E). The main observed effect is an increase in the stability of quartz up temperature and a reduction of the stability of biotite above the solidus. A *T-M*Fe_2O_3 diagram was also calculated (see supplementary material figure E), which suggested a broad range of acceptable values (with the interpreted peak assemblage moving up pressure with lower Fe^{3+} values). Using a value of 30% of Fe^{3+} (Fig. 12c), the interpreted peak assemblage occurs at 650 to 720ºC and 1-3 kbar and is limited at high pressure/low temperature by the loss of titanite and at low pressure/high temperature by the loss of ilmenite, and high T by the presence of melt (Fig. 12c).

- Sample 20-4 (Gonzalito camp; east) contains the interpreted assemblage amphibole + plagioclase + ilmenite + biotite + quartz. Late chlorite replaces biotite and plagioclase is sericitized. A P-T diagram was calculated for this sample using 10% Fe^{3+} (Fig. 12d). On this diagram, the peak assemblage occurs at 550-720 °C and 1-3 kbar and is limited by titanite in at higher pressure, clinopyroxene-in at high temperature and the presence of a second amphibole at low temperature. A *P-M*Fe_2O_3 diagram was calculated to observe the effect of Fe^{3+} concentration on the position of the peak field (see supplementary material figure H). If Fe^{3+} is increased, the peak field occurs at lower pressure, with a maximum pressure of 3 kbar if all the iron is $Fe^{2+.}$ (see supplementary material figure H).

- Sample 22-3 (Puesto El Panchito; central sector) containss the mineral assemblage amphibole + plagioclase + titanite + ilmenite + quartz. Similarly to sample 31/32-3, the peak assemblage occurs only with biotite. However, the modes of biotite are also very low (<2%). The interpreted peak assemblage with biotite occurs at 2.5-3 kbar and 550-700 °C on a P-T diagram with 100% Fe^{2+} (Fig. 12d). This field is bound by ilmenite and titanite stability at high and low pressure respectively. If the amount of Fe^{3+} is increased (supplementary material figures I and J), the location of the peak field moves down-pressure, but the temperature stability range does not change (Figs. 13). If Fe^{3+} is increased by only a small amount, for example to 10% Fe3+, then clinopyroxene stability increases and the interpreted peak field occurs below 2 kbar (see supplementary material figures I and J).

A Venn diagram (Fig. 13) is used to place further constraints on the pressure and temperature conditions by overlaying the peak fields of all the samples. The stability field of the metamafic rocks is roughly estimated between 550 and 730 ºC and below 4 kbar. We consider these results as initial calculations of the P-T conditions since this study lacks mineralogical compositions nor the full composition of the opaque phases. It is clear from the diagrams of Figures 12a-d that the presence of ilmenite in the metamorphic assemblages is decisive in lowering the maximum pressure down to 4 kbar. Therefore, until we can confirm the presence of ilmenite with EPMA, we consider 4 kbar to be the preliminary estimation for the peak pressure conditions.

6. Interpretation and discussion

6.1. Characterization of the main protoliths of the Mina Gonzalito Complex

The lithological assemblage involved in the Mina Gonzalito Complex includes quartz- biotite schists, quartz-biotite-plagioclase gneisses, granitic orthogneisses, metamafic intrusive rocks, minor amphibolites (with mafic and calcsilicatic protoliths), and subordinate carbonate rocks. The metamafic intrusive units were intruded along the S1 or S2 foliation developed in the para and ortho-derived schists and gneisses of the Mina Gonzalito Complex and subsequently folded. Giacosa (1987) proposes a wide distribution for the amphibolites and indicates that the presence of diopside in the west of block (close to Tapera pluton) that coincides with the area of higher metamorphic grade, granitic injection and deformation in the block. In addition, the latest cartography of the Mina Gonzalito (González et al. 2008b; González et al. 2014; Pugliese et al. submitted; this study) reveals that the orthogneisses and synkinematic leucogranites outcrop mostly in the western sector of the block, where they dominate over the sedimentary-derived gneisses. This would suggest a higher-grade metamorphism in the west than in the east. Our study could not perform a systematic work on the para-derived rocks in order to provide evidence for the increase of the metamorphic grade to the west. However, we show that the presence of metamafic protoliths (i.e. banded and massive) are widespread from the west to east of the block, but probably, scattered given their lower volume and considerable dismemberment due to the intense and repeated deformational events during the Permian, Triassic and Jurassic times.

Hereafter, the Mina Gonzalito Complex is reinterpreted as having a larger proportion of (mafic to intermediate) metaigneous protoliths than previously proposed. Several of the metamafic rocks show a transitional variation from banded metamafic rock with diopside layers to more massive levels with more than 50% of clinoamphibole and limited quartz. We interpret the banding as an igneous inherited feature perhaps enhanced by the recrystallization and deformation that occurred during or just after emplacement. In many localities, metamafic rocks show no record of superimposed deformation, suggesting that the mica-rich host (Mina Gonzalito gneiss) could have absorbed the deformation. The protoliths of igneous metamafic rocks are interpreted to be dominated by epizonal rocks of broadly basaltic/ gabbroic composition. It is noteworthy that there are no high-Mg rocks identified within the sequence.

6.2. Petrotectonic setting of the protolith

Following the proposals of Greco et al. (2017) and González et al. (2018), the protoliths of the Nahuel Niyeu Formation and the Mina Gonzalito Complex were mostly associated with a fore-arc tectonic environment with development of a back-arc basin where the El Jagüelito Formation, located to the east (present coordinates), would have been formed. Following these proposals, the Early to mid-Cambrian magmatic arc would be represented by the I-type Tardugno granodiorite orthogneiss (Pankhurst et al. 2014) and the Ordovician tectono-metamorphic event would have affected both basins synchronously at ca. 472 Ma.

Major, trace and rare earth element data indicate that the metamafic rocks are dominantly basaltic in composition with wide variations in MgO contents (5.8 -9.4 wt.%) and Mg# values (Mg#=100×Mg^{+2+}/(Mg^{+2}+ Fe^{+2}_{tot})) between 47 and 69, but a very restricted SiO_2 content, between 45.2 and 52.1 wt.%. K_2O contents are very low (<1.2; in samples with low LOI) and Al_2O_3/TiO_2 ratios are high on average. In addition, these metamafic rocks are characterized by relative enrichment in LILEs and pronounced depletion in HFSEs (e.g., Nb, Ti, Zr, and Hf) (Fig. 11), suggesting that the magmas experienced fractionation and moderate involvement of crustal contamination in the magma source. These geochemical features suggest that these rocks could have been formed either as mid-ocean ridge basalts (MORB), island-arc to transitional basalts (IAT), or in a continental rift environment.

According to Henderson (1984) the average ratio of $(La/Yb)_N$ is greater than 12 at most in continental rift basalts and is lower in environments where oceanic basalts and transitional basalts are produced. In the metamafic rocks of the Mina Gonzalito Complex, the $(La/Yb)_N$ ratio ranges from 0.5 to 2.7, except for the banded metamafic rocks (>12). Moreover, Fitton et al. (1991) characterized basalts erupted during intra-continental extension or incipient rifting as having a Th/Ta ratio >4. This ratio is below 2 in the metamafic rocks from Mina Gonzalito, and characteristic of the island–arc-type rocks. Therefore, the geochemical characteristics of these rocks would not be compatible with a continental rift environment.

Condie (1989) suggested that the Ti/V ratio is less than 30 in island arc tholeiites, and larger than 30 in within-plate basalts. The Ti/V average ratio for the metamafic rocks of Gonzalito Mine is below 25, with two outliers, samples PG6 and P8, that were interpreted to be cumulates (Figure 14a). The samples show values that correspond to those associated with magmatic arc to MOR and back-arc basalts. In Figure 14b, c two other trace-elements relations, such as 2*Nb, Zr/4 and Y, (Meschede 1986) and La/10, Y/15 and Nb/8 (Cabanis and Lecolle, 1989) triangles also suggest that they have a volcanic back-arc affinity. Assuming that the crustal input in arc magmatism can be proxied with the Th/Yb versus Nb/Yb (Fig. 14d), as proposed by Pearce (2008), the metamafic rocks of the MGC are shifted above the mantle array, suggesting they are mantle derived and have experienced magma-crust interaction.

Moreover, when several incompatible element ratios such as Zr/Y (1.9-3.2), Zr/Nb (>14), Zr/Y (<3.2), Nb/La (<1), $(Ce/Y)_N$ (0.6-1.7), Na/La (0.4-1.0) are compared with MOR-type basalt, ocean island basalts and high-alumina calc-alkaline and island-arc tholeiites, the metamafic rocks of Mina Gonzalito are more similar to those of transitional between the Normal to slightly enriched MOR and island arc-type subduction related basalts (see table in the Supplementary material B).

Gribble et al. (1996, 1998) suggested that the tectonic environment, which not only may produce MORB-like basalt but also may produce arc volcanic-like basalt signatures, is a back-arc basin. Therefore, we interpret that the protoliths of the metamafic rocks were emplaced in a back-arc tectonic setting.

6.3. Interpretation of the P-T phase diagrams

The studied samples have high variant assemblages resulting in large fields on the P-T diagram. All the samples must have experienced the same metamorphic event and come from closely spaced locations. Therefore, it could be possible to use their variable compositions to further constrain their P-T conditions. In Figure 13, the peak fields of all these samples have been overlaid in a Venn diagram. The presence of ilmenite and titanite in samples 31/32-3 and P8-2B constrains the temperature to 650-730 ºC, and all the samples indicate low pressure (between 1-4 kbar). The protolith would likely be (hornblende) gabbros, implying a water enriched magma and suggesting lower than MORB crystallization temperatures. These temperatures within the range of calculated temperatures for the re-equilibration. Textural evidence indicates that the composition of the metamafic rocks would not have been very reactive to metamorphism and only recrystallized in a few cases (dependent on degree of deformation and presence of H_2O).

Altogether, the results of the pseudosections would suggest low pressure (less than 4 kbar) and intermediate temperature (640-730° C) conditions compatible with emplacement and recrystallization of water-rich gabbroic intrusions within the Mina Gonzalito Complex. These conditions may not correspond to those of the garnet-biotite paragneiss, which has not been the subject of a metamorphic study but has been suggested to have achieved higher-P conditions (González et al. 2008b). Indicating that the low P, higher T conditions of the mafic rocks may have developed after, the higher-P amphibolite facies conditions dated at ~472 Ma (Pankhurst et al. 2006). This anticlockwise evolution would also be consistent with a back-arc tectonic setting, however this interpretations relies on further P-T modelling of the gneisses and schists of Mina Gonzalito in order to confirm their peak conditions and is a forthcoming step to understand the metamorphic history of the basement.

6.4. Timing of the sedimentation, metamorphism, magmatism and deformation and favored chronology

Despite the limited outcrops of metamafic rocks, metagranites and gneisses in the Early Paleozoic basement of the North Patagonian Massif, their origin, evolution and tectonic significance are key aspects to complete the puzzle of the evolution of northern Patagonia and support evidence in favour or against the plethora of hypothesis regarding its origin. Previous geochronological data states that the metamorphic peak (M1 or M2) was recorded at 472 ± 5 Ma (U-Pb SHRIMP2 in zircon; Pankhurst et al. 2006) in a biotite-garnet paragneiss around Gonzalito mine. More recently, the age of the metamorphic peak was further confirmed in another paragneiss located *ca* 7 km to the northwest of the Mina Gonzalito mine (~472 Ma U-Pb zircon LA-ICP-MC; Greco et al., 2014). The depositional age for the protolith of the paragneiss should be younger than 518 ± 6 Ma according to the ages of the inherited zircon cores reported by Pankhurst et al. (2006) (Fig. 14). Comparable maximum depositional ages, between 510 and 515 Ma, were obtained in the low-grade metaclastic protoliths of the Nahuel Niyeu Formation (Greco et al. 2017; Pankhurst et al. 2006; Rapalini et al. 2013) and in the metaigneous layers interlayered within the El Jagüelito low-grade metasedimentary rocks (González et al. 2018). However, the presence of metamorphic enclaves of El Jagüelito Formation in the granites and tonalites of the shallow crustal Punta Sierra Plutonic Complex, accurately dated at 476 ± 5 Ma and 475 ± 2 Ma, implies that the metamorphic event recorded in the El Jagüelito Formation (M1) must be synchronous or older than the age of the magmatism. K-Ar muscovite dating of a hornfels in El Jagüelito Formation (post-M1) yielded 459 ± 9 Ma. Therefore, it would reasonable that the metamorphic event (M1) could be older than that registered in Mina Gonzalito.

The Early Ordovician age of the metamorphic peak of biotite-garnet gneisses in the Mina Gonzalito Complex (i.e., M2?) was obtained by Pankhurst et al. (2006) from the rims of inherited zircon grains, assuming that these rims were produced during amphibolite facies metamorphic conditions. This age overlaps with that of the Peñas Blancas granite dated at 471 ± 2 Ma with U-Pb zircon SHRIMP dating (García et al. 2012) close to Gonzalito mine (Fig.2). This pluton hosts a peraluminous, garnet and muscovite bearing-granite facies compatible with those generated by partial melting of metapelitic rocks.

Varela et al. (2011) dated several acidic ortho-derived rocks within the Mina Gonzalito Complex not far from Puesto Dragón, obtaining a U-Pb SHRIMP crystallization age of 492 ± 6 Ma for the crystallization of a granodioritic orthogneiss and a Rb-Sr cooling age, calculated with a composite WR, biotite and K-feldspar isochron that yielded 257 ± 4 Ma, suggesting that this age corresponds to a Permian episode of deformation or metamorphism (Varela et al. 2009) (Fig. 14). Conversely, in the surroundings of the Mina Gonzalito mineshaft they obtained a Rb-Sr cooling age of 452 ± 29 Ma (WR-mineral isochron) from of a foliated leucogranite (e.g., “tonalitic gneiss” from Varela et al. 1997). This observation allowed Varela et al. (2011) to propose a dual cooling evolution of the complex: a faster (Ordovician) exhumation-time path for the eastern portion and a slower (Permian) trajectory for the westernmost part.

Metamafic lenses in the MGC are mostly metaigneous bodies that were intruded along S_1 or S_2 developed in the para and ortho-derived gneisses of the Mina Gonzalito Complex and subsequently deformed, having variably experienced the effects of D_{n+1}. Having no evidence of high grade paragenesis, the metamorphism in the metamafic rocks would be evidenced by recrystallization and re-equilibrium of the magmatic paragenesis. Thus, their protoliths were not quite different in mineralogical composition from the original rock, i.e., hornblende gabbro. Even though there are no absolute ages for the metamafic rocks, the absence of a thermal aureole, the large grainsize of the intrusions and the fact that they are folded together with their host during $D_{n+}2$ suggests that the protoliths of the metamafic rocks (hornblende-gabbros) intruded within an already metamorphosed and deformed ($M_{n+}1$-$D_{n+}1$) metaclastic and metaigneous package of the Mina Gonzalito Complex. González et al. (2008b) interpreted “amphibolite layers” intercalated in the paragneisses and schists of the Mina Gonzalito Complex as pre-kinematic, mafic igneous flows, and also considered them as the higher metamorphic equivalents of the sills and the lava flows of the Nahuel Niyeu Formation. Recently, Greco et al. (2015) obtained a set of U-Pb zircon ages of a “(…) metagranite differentiate of a metagranodiorite facies of a metagranodiorite-gabbro/diorite composite sill (…)” interlayered with the Nahuel

Niyeu Formation close to Aguada Cecilio (50 km to the North of Mina Gonzalito). These authors considered the metagranite as an *in situ* magmatic differentiate product from a gabbroic sill (Fig. 14) and calculated a concordia age at 513.6 ± 3.3 Ma, equivalent to the maximum depositional age of its host (~515 Ma; Greco et al. 2017). These authors further proposed that the timing of the D_1-D_2-M_1 tectonometamorphic event in the Nahuel Niyeu Formation is constrained between the emplacement of these sills and post-D2 microgranodiorite dikes. The microgranodiorite dikes could belong to thePunta Sierra Plutonic Complex (crystallization age ~476 Ma; Pankhurst et al. 2006) or to the Late Permian plutonic complexes, as suggested by the K-Ar biotite age of 257 ± 7 Ma of Varela et al. (2001). Further evidence is found in the Valcheta pluton that clearly intrudes the already metamorphosed rocks of Nahuel Niyeu Formation in Valcheta area, and whose mica Ar-Ar and K-Ar cooling ages are bracketed between 470-450 Ma (López de Luchi et al. 2008; Tohver et al. 2008; Gozálvez 2009).

Therefore, the D_1-D_2-M_1 tectonometamorphic event in the Valcheta to Aguada Cecilio area can be constrained between the crystallization age assigned to the “granitic differentiate of mafic sills and the ca. 470-450 Ma cooling of the Valcheta Pluton (Fig. 14)..Several younger highly concordant $^{206}Pb/^{238}U$ ages between 487 and 450 Ma obtained for the granitic differentiate were interpreted as a product of Pb loss due to coeval metamorphism and deformation (D_1-D_2, M_1). A review of the dataset of Greco et al. (2015) allows the calculation of a younger concordia age for the granite sill at 460.8 ± 3.6 Ma (N=4; MSWD 0.15 and common Pb ≤ 2%). This age is more consistent with the fact that these coarse-grained rocks require burial before the in situ melting of the host rock could occur. Dehydration melting reaction of the host could explain the ~515 Ma inheritance within the “granitic differentiate”.

Combining the evidence in the Nahuel Niyeu Formation and the Mina Gonzalito Complex, we infer that the metamafic rocks of the Mina Gonzalito Complex are equivalent as already suggested by Greco et al (2015) but their magmatic crystallization age should be Ordovician The onset of widespread intrusive mafic and ultramafic bodies (i.e. peridotites; Greco et al. 2015) within a shallow crust as, perhaps, the roots of the Early Ordovician magmatic arc would explain the increase in the thermal gradient and high T/P conditions, and possibly, a partial melting event affecting a probably already M1-metamorphosed complex.

Further folding and local dynamic retrogression and faulting would have occurred during the onset of the Permian, Triassic, and later Jurassic shallow magmatism (i.e. Pailemán Plutonic Complex and Treneta and Marifil volcanic complexes)

We recalculated a WR Rb-Sr isochron built with data taken out of a small dataset of metamafic rocks (amphibolites) from Tres Marías mine and Gonzalito mines (P30-5; P11-1; P5-3; Aragón et al. 1999b) that yielded 267 ± 13 Ma (MSWD 0.008; probability 0.93) -using the Model-1 solution of Isoplot 4.15 (Ludwig 2000). The initial $^{87}Sr/^{86}Sr$ ratio calculated out of the isochron (0.70011 ± 0.0013) is lower than values expected for the Depleted Mantle, suggesting that the data is showing a disturbance of the Rb-Sr system rather than a primary cooling age.

The Rb-Sr cooling age for the metamafic rocks (e.g. ∼265 Ma) is within analytical error of other Late Permian cooling ages in the area, such as the mica-ages of the Tapera Granite ($^{40}Ar/^{39}Ar$ biotite of 264 ± 2 Ma; Grecco and Gregori 2011) and the María Teresa Granite ($^{40}Ar/^{39}Ar$ muscovite of 261 ± 2 Ma; Grecco and Gregori 2011) and its hosting paragneiss (^{40}K-^{40}Ar biotite of 266 ± 10 Ma; Llamas 1995). Our field observations agree with those of Giacosa et al. (1993), both granite plutons are deformed concordantly with the large-scale structure of the metamorphic host, but they do not produce a thermal aureole in their hosting gneisses. An identical age interval (260-265 Ma) of granite emplacement is given in the Tembrao river, 30 km to the North of Mina Gonzalito, where the Pailemán Plutonic Complex (Giacosa 1993) intrudes the red-biotite bearing schists of the Mina Gonzalito Complex parallel to the Sn+1 (synkinematically). Crystallization and mica-cooling ages of the synkinematic Arroyo Tembrao granodioritic orthogneiss ($^{39}Ar/^{40}Ar$ biotite of 266 ± 2 Ma; Grecco and Gregori 2011, unpublished data) and of a N-S vertical undeformed aplopegmatitic dyke (^{40}K-^{40}Ar muscovite of 264 ± 6 Ma; López de Luchi et al. 2008) that cuts across the host rocks of both the Arroyo Tembrao Granodiorite and the Paileman Granite constrain the emplacement and D3 deformation as Late

Permian (as observed earlier by Greco 2015 in the Aguada Cecilio area). The aplopegmatite dyke swarm (260-255 Ma) is notably undeformed and crosscuts the Sn+1 deformation of the basement. A NNW-SSE trending vertical muscovite-bearing aplopegmatite dyke swarm can be tracked from Tembrao river to the centre to the Mina Gonzalito area. Another piece of significant evidence in this puzzle are of two samples of an undeformed pegmatite dyke taken from La Leona mine, 3 km to the NE of Mina Gonzalito camp, whose muscovite grains are aged 249 ± 9 Ma (^{40}K-^{40}Ar on muscovite; Genovese 1996). Remarkably, Arroyo Tembrao granodiorites contain metamorphic enclaves of the host, suggesting that the Sn+1 penetrative structure, and possibly thermal reheating, might have had ended by *ca.* 250 Ma. The larger analytical spread of the Late Permian mica cooling ages, particularly the biotite ages, is partly attributed to reheating (and opening of low-temperature isotopic systems) and hydrothermal alteration of the basement during the intrusion of the Paileman Plutonic Complex, and potentially also related to the exhumation of the western part of the Mina Gonzalito Complex where most of these ages are recorded.

In contrast with the granitic synkynematic María Teresa and Tapera plutons, the body of the Santa Rosa Diorite crosscuts the biotite-muscovite gneisses of the Mina Gonzalito Complex. The pluton does not show significant evidence of penetrative deformation, except close to the decameter scaled S-C shear zones (probably D3 or D4 of González et al., 2008b). The Santa Rosa pluton remains undated. However, the diorites can be assigned to be Permian based on its plausible correlation with the more mafic terms of the granodiorites of the La Verde pluton (Giacosa 1997; Busteros et al. 1998; García et al. 2014), outcropping 25 km to west of Estancia Santa Rosa, and 12 km to the east of Los Berros. Both intrusions display identical petrographical (hornblende-biotite and accessory mineralogy; the presence of mafic microgranular enclaves), geochemical (slightly negative Eu/Eu* anomaly, large La/YbN ratios >7) and structural (undeformed) features. La Verde pluton is dated at 261 ± 2 Ma (U-Pb zircon SHRIMP; García et al. 2014). A ^{40}K-^{40}Ar cooling age of biotites from the same body determined that the system cooled at 253 ± 9 Ma (Busteros et al. 1998). The La Verde pluton was correlated with the granodiorites and granites of the Navarrete (283-275 Ma; Martínez Dopico et al. 2017; Pankhurst et al. 2006) and Yaminué (260-245 Ma; (Chernicoff et al. 2013; Martínez Dopico et al. 2017; Pankhurst et al. 2014) plutonic complexes outcropping to the north and forming, together with the Pailemán Plutonic Complex, the Late Permian to Early Triassic magmatic belt of the North Patagonian Massif (Ramos, 2008).

Overall, the cooling age homogeneity indicates that the thermal effects of Permian igneous activity were localized, typical of higher crustal levels, whereas age homogeneization in the wake of crustal thickening and thermal relaxation would have been expected to occur along the fault and shear zones.

Therefore, we can conclude that the tectonometamorphic event (M2) affected the basement of the Mina Gonzalito Complex occurred during the Early Ordovician producing high T/P metamorphism, partial melting and intrusion of bimodal magmatism, with gabbros to S-type granites. Another significant thermal event, represented in the Gonzalito area by the Santa Rosa Diorite, affected the crust during the Late Permian at ~ 260-250 Ma causing magmatism and deformation in the upper crustal levels, as recorded in the northeastern North Patagonian Massif (López de Luchi et al. *in press*).

7. Final considerations

- The majority of the metamafic rocks of the Mina Gonzalito Complex show a variety of textures compatible with a mafic igneous protolith such as a hornblende-gabbro or hornblendite. Three main paragenesis were found: diopside + clinoamphibole + plagioclase; clinoamphibole + plagioclase; and clinoamphibole + plagioclase + biotite. They are distributed throughout the complex, from the María Teresa mine in the west to the Gonzalito mine camp in the east.
- Geochemical data suggest that the metamafic rocks have transitional chemical characteristics between MOR basalts and island arc tholeiites. This study proposes that the protolith of the metamafic igneous rocks was emplaced in the magmatic arc domain, probably in an intracontinental back-arc basin.

- Even though the age of emplacement of the metamafic protoliths has not been yet constrained, we suggest that their emplacement would be occurred after or during the 472 ± 5 Ma tectonometamorphic event.
- The peak conditions of M2 can be reconciled with a high-temperature event (up to 730 ºC) brought to this crustal level by the metamafic intrusions, explaining the partial melting in the biotite-bearing schists though biotite-dehydration melting reactions.
- Santa Rosa Diorite shows different geochemical characteristics compared to the metamafic rocks interlayered within the Mina Gonzalito Gneiss and probably is Permian in age.

Acknowledgements

We would like to evoke the memory of Dr. Luis Dalla Salda and Dr. E. Linares who collected the samples for this study. We thank Agencia Nacional de Promoción Científica y Tecnológica (ANPCyT) for the grants PICT2016-3148 and PICT2016-2188.

References

Aragón, E., Dalla Salda, L., López de Luchi, M.G., Benialgo, A., Pezzotti, C., 1999a. El distrito polimetálico Gonzalito, Río Negro, in: Recursos Minerales de La República Argentina, Instituto de Geología y Recursos Minerales. Buenos Aires, pp. 373–383.

Aragón, E., Dalla Salda, L., Varela, R., Benialgo, A., 1999b. Jurassic resetted ages of Gonzalito Sedex Deposit, Northeastern Patagonia. II South American Symposium on Isotope Geology, 7-10.

Boynton, W.V., 1984. Cosmochemistry of the rare earth elements: meteorite studies, in: Henderson, P. (Ed.), Rare Earth Element Geochemistry. Elsevier, pp. 62–114.

Busteros, A., Giacosa, R., Lema, H., 1998. Hoja Geológica 4166-IV, Sierra Grande. Provincia de Río Negro. Boletín 241. Instituto de Geología y Recursos Minerales, Servicio Geológico Minero Argentino, Buenos Aires.

Cabanis, B., Lecolle, M., 1989. Le diagramme La/10-Y/15-Nb/8: un outil pour la discrimination des séries volcaniques et la mise en évidence des processus de mélange et/ou de contamination crustale. Comptes rendus de l'Académie des sciences.Série 2, Mécanique, Physique, Chimie, Sciences de l'univers, Sciences de la Terre 309, 2023–2029.

Chappell, B.W., White, A.J.R., 2001. Two contrasting granite types: 25 years later. Aust. J. Earth Sci. 48, 489–500. https://doi.org/10.1046/j.1440-0952.2001.00882.x

Chernicoff, C.J., 1994. Estructura del basamento cristalino del área Yaminue-Nahuel Niyeu, macizo nordpatagónico, Provincia de Río Negro. (PhD Thesis). Universidad de Buenos Aires, Buenos Aires.

Chernicoff, C.J., Caminos, R., 1996. Estructura y relaciones estratigráficas de la Formación Nahuel Niyeu, MAcizo Norpatagónico oriental, provincia de Río Negro. Rev. Asoc. Geológica Argent. 51, 201–212.

Chernicoff, C.J., Zappettini, E.O., Santos, J.O.S., McNaughton, N.J., Belousova, E., 2013. Combined U-Pb SHRIMP and Hf isotope study of the Late Paleozoic Yaminué Complex, Rio Negro Province, Argentina: Implications for the origin and evolution of the Patagonia composite terrane. Geosci. Front. 4, 37–56. https://doi.org/10.1016/j.gsf.2012.06.003

Condie, K.C., 1989. Geochemical changes in basalts and andesites across the Archean-Proterozoic boundary: Identification and significance. Lithos 23, 1–18. https://doi.org/10.1016/0024-4937(89)90020-0

Cortés, J., 1981. El sustrato precretácico del extremo nordeste de la provincia de Chubut. Rev. Asoc. Geológica Argent. 36, 217–235.

Cox, K.G., Bell, J.D., Pankhurst, R.J., 1979. The interpretation of igneous rocks. Allen and Unwin, London.

De Capitani, C., Petrakakis, K., 2010. The computation of equilibrium assemblage diagrams with Theriak/Domino software. Am. Mineral. 95, 1006–1016. https://doi.org/10.2138/am.2010.3354

Dalla Salda, L., Aragón, E., Benialgo, A., Pezzoti, C., 2003. Una plataforma calcárea en el Complejo Mina Gonzalito, provincia de Río Negro. Revista de la Asociación Geológica Argentina 58: 209-217

Del Mónaco, A., 1971. Geología económica de los niveles 110 y 140 de la mina Gonzalito (provincia de Río Negro), República Argentina. Rev. Asoc. Geológica Argent. 26, 57–66.

Droop, G.T.R., 1987. A general equation for estimating Fe 3+ concentrations in ferromagnesian silicates and oxides from microprobe analyses, using stoichiometric criteria. Mineralogical Magazine, 51, 431-435.

Fitton, J.G., James, D., Leeman, W.P., 1991. Basic magmatism associated with Late Cenozoic extension in the western United States: compositional variation in space and time. J. Geophys. Res. 96, 13696–13711.

Gale, A., Dalton, C.A., Langmuir, C.H., Su, Y., Schilling, J.-G., 2013. The mean composition of ocean ridge basalts: MEAN MORB. Geochem. Geophys. Geosystems 14, 489–518. https://doi.org/10.1029/2012GC004334

García, V.A., González, S., Tassinari, C.C.G., Sato, K., Sato, A.M., González, P.D., Varela, R., 2014. Geoquímica y geocronología del Plutón La Verde, Macizo Nordpatagónico, provincia de Río Negro, in: Actas. Presented at the XIX Congreso Geológico Argentino, Córdoba, pp. 373–374.

García, V.A., Sato, A.M., González, P.D., Varela, R., González, S.N., Greco, G.A., 2012. Geología y geoquímica del plutón Peñas Blancas, Macizo Norpatagónico, Río Negro, in: Actas. Presented at the 2nd Simposio sobre Petrología Ígnea y Metalogénesis Asociada, San Luis.

Genovese, S., 1995. Geología y geocronología del área de la mina La Leona, departamento San Antonio, provincia de Río Negro. Trabajo final de licenciatura, Universidad de Buenos Aires, (inédita), 76 p., Ciudad Autónoma de Buenos Aires.

Giacosa, R., 1987. Caracterización de un sector del basamento metamórfico-migmatítico en el extremo suroriental del Macizo Norpatagónico., in: Actas. Presented at the X Congreso Geológico Argentino, San Miguel de Tucumán, pp. 51–54.

Giacosa, R.E., 1997. Geología y petrología de las rocas pre-cretácicas de la region de sierra Pailemán, Provincia de Rio Negro, in: Actas 4. Presented at the 12° Congreso Geológico Argentino and 2° Congreso de exploración de Hidrocarburos, pp. 113–119.

González, P.D., Sato, A.M., Varela, R., Greco, A.G., Naipauer, M., Llambías, E.J, Basei, M., 2014. Metamorfismo y estructura interna de la Formación El Jagüelito en el Arroyo Salado inferior, Macizo Norpatagónico, Río Negro. XIX Congreso Geológico Argentino T8-22.

González, P.D., Sato, A.M., Naipauer, M., Varela, R., Basei, M., Sato, K., Llambías, E.J., Chemale, F., Dorado, A.C., 2018. Patagonia-Antarctica Early Paleozoic conjugate margins: Cambrian synsedimentary silicic magmatism, U-Pb dating of K-bentonites, and related volcanogenic rocks. Gondwana Res. 63, 186–225. https://doi.org/10.1016/j.gr.2018.05.015

González, P.D., Sato, A.M., Varela, R., Llambías, E.J., Naipauer, M., Basei, M.A.S., Campos, H., Greco, G.A., 2008b El Molino Pluton: A granite with regional metamorphism within El Jagüelito Formation, North Patagonian Massif. VI South AMerican Symposium on Isotope Geology, San Carlos de Bariloche, E-files 4p.

González, P.D., Varela, R., Sato, A.M., Llambías, E.J., 2008b. Dos fajas estructurales distintas en el Complejo Mina Gonzalito, Río Negro. XVII Congr. Geológico Argent. 847–848. https://doi.org/10.1142/s0218927515500091

González, S.N., Greco, G.A., González, P.D., Sato, A.M., Llambías. E., Varela, R., Basei, M.A.S., 2014. Geología, petrografía y edad U-Pb de un enjambre longitudinal NO-SE de diques del Macizo Nordpatagónico Oriental, Río Negro. Revista de la Asociación Geológica Argentina 71:174-183

González, S.N., Greco, G.A., Sato, A.M., Llambías, E.J., Basei, M.A.S., González, P.D., Díaz, P.E., 2017. Middle Triassic trachytic lava flows associated with coeval dyke swarm in the North Patagonian Massif: A postorogenic magmatism related to extensional collapse of the Gondwanide orogen. J. South Am. Earth Sci. 75, 134–143. https://doi.org/10.1016/j.jsames.2017.02.007

Gozálvez, M.R., 2009. Petrografía y edad40Ar/39Ar de leucogranitos peraluminosos al oeste de valcheta. macizo nordpatagónico (Río Negro). Rev. Asoc. Geol. Argent. 64, 285–294.

Grecco, L.E., Gregori, D.A., 2011. Geoquímica y geocronología del Complejo Plutónico Pailemán, Cormarca Nordpatagónica, Provincia de Río Negro, in: Actas. Presented at the XVIII Congreso Geológico Argentino, Neuquén, pp. 91–92.

Grecco, L.E., Gregori, D.A., Rapela, C.W., Pankhurst, R.J., Labudia, C.H., 1994. Peraluminous granites in the Northeastern sector of the North Patagonian Massif, in: Actas II. Presented at the 8 Congreso Geológico Chileno, pp. 1354–1359.

Greco, G.A., González, P.D., González, S.N., Sato, A.M., Basei, M.A.S., Tassinari, C.C.G., Sato, K., Varela, R., Llambías, E.J., 2015. Geology, structure and age of the Nahuel Niyeu Formation in the Aguada Cecilio area, North Patagonian Massif, Argentina. J. South Am. Earth Sci. 62, 12–32. https://doi.org/10.1016/j.jsames.2015.04.005

Greco, G.A., González, S.N., Sato, A.M., González, P.D., Basei, M.A.S., Llambías, E.J., Varela, R., 2017. The Nahuel Niyeu basin: A Cambrian forearc basin in the eastern North Patagonian Massif. J. South Am. Earth Sci. 79, 111–136. https://doi.org/10.1016/j.jsames.2017.07.009

Greco, G.A., González, S.N., Sato, A.M., González, P.D., Llambías, E.J., Basei, M.A.S., 2014. Nueva datación en circones detríticos para el Complejo Mina Gonzalito, Provincia De Río Negro, in: Actas XIX Congreso Geológico Argentino. Presented at the XIX Congreso Geológico Argentino, Córdoba, p. 2.

Green, E.C.R., White, R.W., Diener, J.F.A., Powell, R., Holland, T.J.B., Palin, R.M., 2016. Activity-composition relations for the calculation of partial melting equilibria in metabasic rocks. J. Metamorph. Geol. 34, 845–869. https://doi.org/10.1111/jmg.12211

Hastie, A.R., Kerr, A.C., Pearce, J.A., Mitchell, S.F., 2007. Classification of Altered Volcanic Island Arc Rocks using Immobile Trace Elements: Development of the Th–Co Discrimination Diagram. J. Petrol. 48, 2341–2357. https://doi.org/10.1093/petrology/egm062

Henderson, P., 1984. Rare Earth Element Geochemistry, Developments in Geochemistry. Elsevier, Amsterdam.

Holland, T.J.B. & Powell, R., 2003. Activity-composition relations for phases in petrological calculations: an asymmetric multicomponent formulation. Contributions to Mineralogy and Petrology, 145, 492-501.

Holland, T.J.B. & Powell, R., 2011. An improved and extended internally consistent thermodynamic dataset for phases of petrological interest, involving a new equation of state for solids. Journal of Metamorphic Geology, 29, 333-383

Irving, T.N., Baragar, W.R.A., 1971. A Guide to the Chemical Classification of the Common Volcanic Rocks. Can. J. Earth Sci. 8, 523–548.

Janousek, V., Farrow, C.M., Erban, V., 2006. Interpretation of whole-rock geochemical data in igneous geochemistry: introducing Geochemical Data Toolkit (GCDkit). J. Petrol. 47, 1255–1259.

Jorgensen, T.R.C., Tinkham, D.K., Lesher, C.M., 2019. Low-P and high-T metamoprhism of basalts: Insights from the Sudbury impact melt sheet aureole and thermodynamic modelling. Journal of Metamorphic Geology 37:271-313.

Linares, E., Parica, C., Parica, P. D., 1985. Catálogo de edades radiométricas determinadas para la República Argentina. Asociación Geológica Argentina, Buenos Aires.

Llamas, O., 1995. Geología y geocronología del área de Tres Marías, Departamento de San Antonio, Provincia de Río Negro. Universidad de Buenos Aires, Buenos Aires.

López de Luchi, M., Wemmer, K., Rapalini, A.E., 2008. The Cooling History Of The North Patagonian Massif: First Results For The Granitoids Of The Valcheta Area, Río Negro, Argentina, in: Abstracts. Presented at the VI South American Symposium on

Isotope Geology, Bariloche, p. 4.

López de Luchi, M.G., Martínez Dopico, C., Rapalini, A.E., Rapela, C.W., Pankhurst, R.J., 2014. Petrology of the Ordovician I- And S-Type Granitoids of the NE sector of the North Patagonian Massif, in: XIX Congreso Geológico Argentino. pp. S21–28. https://doi.org/10.5027/andgeoV40n2-aXX.Villarosa

López de Luchi, M.G., Martínez Dopico, C., Rapalini, A., 2020. The Permian to Early Triassic granitoids of Nahuel Niyeu - Yaminué area, Northern Patagonia: geochemistry, microstructures and emplacement conditions. Journal of South American Earth Sciences (submitted)

Ludwig, K., 2000. Users manual for Isoplot/Ex: a geochronological toolkit for Microsoft Excel. Berkeley Geochronology Center Spec. Publ.. 1a. 53.

Luppo, T., López de Luchi, M.G., Rapalini, A.E., Martínez Dopico, C.I., Fanning, C.M., 2018. Geochronologic evidence of a large magmatic province in northern Patagonia encompassing the Permian-Triassic boundary. J. South Am. Earth Sci. 82, 346–355. https://doi.org/10.1016/j.jsames.2018.01.003

Martínez Dopico, C., López de Luchi, M., Rapalini, A.E., 2014. Petrography and mineral chemistry of the early paleozoic metamorphic basement north of Valcheta town, Río Negro, in: XIX Congreso Geológico Argentino. pp. S21–36.

Martínez Dopico, C.I., López de Luchi, M.G., Rapalini, A.E., Fanning, C.M., Antonio, P.Y.J., 2019. Geochemistry and geochronology of the shallow-level La Esperanza magmatic system (Permian-Triassic), Northern Patagonia. J. South Am. Earth Sci. 96, 102347. https://doi.org/10.1016/j.jsames.2019.102347

Martínez Dopico, C.I., López de Luchi, M.G., Rapalini, A.E., Kleinhanns, I.C., 2011. Crustal segments in the North Patagonian Massif, Patagonia: An integrated perspective based on Sm-Nd isotope systematics. J. South Am. Earth Sci. 31, 324–341. https://doi.org/10.1016/j.jsames.2010.07.009

Martínez Dopico, C.I., López de Luchi, M.G., Wemmer, K., Luppo, T., Rapalini, A.E., Buceta, G., 2017a. Geochronology and geochemistry of hybrid quartz-monzogabbro to granodiorite stocks of the Valcheta Plutonic Complex, Northeastern Patagonia, in: Ibañez, L.M., Grosse, P., Báez, M. (Eds.), XX Congreso Geológico Argentino. San Miguel de Tucumán, pp. 76–78.

Martínez Dopico, C.I., Tohver, E., López de Luchi, M.G., Wemmer, K., Rapalini, A.E., Cawood, P.A., 2017b. Jurassic cooling ages in Paleozoic to early Mesozoic granitoids of northeastern Patagonia:40Ar/39Ar,40K-40Ar mica and U–Pb zircon evidence. Int. J. Earth Sci. 106, 2343–2357. https://doi.org/10.1007/s00531-016-1430-0

Meschede, M., 1986. A method of discriminating between different types of mid-ocean ridge basalts and continental tholeiites with the Nb-Zr-Y diagram. Chem. Geol. 56, 207–218. https://doi.org/10.1016/0009-2541(86)90004-5

Miyashiro, A., 1974. Volcanic Rock Series in Island Arcs and Active Continental Margins. Am. J. Sci. 274, 321–355.

Ohta, T. & Arai, H. (2007) Statistical empirical index of chemical weathering in igneous rocks: a new tool for evaluating the degree of weathering. Chemical Geology 240,280–297v

Pankhurst, R.J., Rapela, C.W., Fanning, C.M., 2001. The Mina Gonzalito Gneiss: Early ordovician metamorphism in northern Patagonia, in: Extended Abstracts. Presented at the Third South American symposium on isotope geology, Pucón, pp. 604–607.

Pankhurst, R.J., Rapela, C.W., Fanning, C.M., Márquez, M., 2006. Gondwanide continental collision and the origin of Patagonia. Earth-Sci. Rev. 76, 235–257. https://doi.org/10.1016/j.earscirev.2006.02.001

Pankhurst, R.J., Rapela, C.W., López De Luchi, M.G., Rapalini, A.E., Fanning, C.M., Galindo, C., 2014. The Gondwana connections of northern Patagonia. J. Geol. Soc. 171, 313–328. https://doi.org/10.1144/jgs2013-081

Pankhurst, R.J., Riley, T.R., Fanning, C.M., Kelley, S.P., 2000. Episodic Silicic Volcanism in Patagonia and the Antarctic Peninsula: Chronology of Magmatism Associated with the Break-up of Gondwana. J. Petrol. 41, 605–625. https://doi.org/10.1093/petrology/41.5.605

Pearce, J.A., 1982. Trace element characteristics of lavas from destructive plate boundaries, in: Andesites: Orogenic Andesites and Related Rocks. John Wiley & Sons, Chichester, pp. 525–548.

Pearce, J.A., 2008. Geochemical fingerprinting of oceanic basalts with applications to ophiolite classification and the search for Archean oceanic crust. Lithos 100: 14-48 doi:10.1016/j.lithos.2007.06.016

Peccerillo, A., Taylor, S.R., 1976. Geochemistry of eocene calc-alkaline volcanic rocks from the Kastamonu area, Northern Turkey. Contrib. Mineral. Petrol. 58, 63–81. https://doi.org/10.1007/BF00384745

Pugliese, F., Dahlquist, J.A., Pugliese, L.E., 2019. Manifestaciones epitermales auríferas de baja sulfuración en el Distrito Polimetálico Gonzalito, Provincia de Río Negro, República Argentina, in: Acta de Resúmenes. Presented at the XIII Congreso de Mineralogía, Petrología Ígnea y Metamórfica, y Metalogénesis, Córdoba, pp. 368–369.

Ramos, V.A., 2008. Patagonia: A paleozoic continent adrift? J. South Am. Earth Sci. 26, 235–251. https://doi.org/10.1016/j.jsames.2008.06.002

Ramos, V.A., 1975. Geología del sector oriental del Macizo Nordpatagónico entre Aguada Capitán y la Mina Gonzalito, provincia de Río Negro. Rev. Asoc. Geológica Argent. 30, 274–285.

Rapalini, A.E., de Luchi, M.L., Tohver, E., Cawood, P.A., 2013. The South American ancestry of the North Patagonian Massif: geochronological evidence for an autochthonous origin? Terra Nova 25, 337–342. https://doi.org/10.1111/ter.12043

Rapalini, A.E., López de Luchi, M.G., Martínez Dopico, C., Lince Klinger, F., Giménez, M., Martínez, P., 2010. Did Patagonia collide with Gondwana in the late Paleozoic? Some insights from a multidisciplinary study of magmatic units of the North Patagonian Massif. Geol. Acta 8, 349–371. https://doi.org/10.1344/105.000001577

Rapela, C.W., Caminos, R., 1987. Geochemical characteristics of the upper Paleozoic magmatism in the eastern sector of the North Patagonian Massif. Rev. Bras. Geocienc. 17, 535–543.

Rosenman, H.L., 1972. Geología de la región de Arroyo Los Berros (vertiente oriental de la Meseta de Somuncura), Provincia de Río Negro, República Argentina. Rev. Asoc. Geológica Argent.

Rustán, J., Cingolani, C.A., Cicadi, A., Uriz, N.J., 2013. Lower Silurian trilobites from the Northern Ptagonia Sierra Grande Formation. Ameghiniana 50, R68.

Saunders, A.D., Tarney, J., 1979. The geochemistry of basalts from a back-arc spreaading centre in the East Scotia Sea. Geochim. Cosmochim. Acta 43, 555–572.

Sun, S., 1980. Lead isotopic study of young volcanic rocks from midocean ridges, ocean islands and island arcs. Philosophical Transactions of the Royal Society of London, Series A 297, 409–445.

Sun, S. -s., McDonough, W.F., 1989. Chemical and isotopic systematics of oceanic basalts: implications for mantle composition and processes. Geol. Soc. Lond. Spec. Publ. 42, 313–345. https://doi.org/10.1144/GSL.SP.1989.042.01.19

Taylor, J., Nicoli, G., Stevens, G., Frei, D., & Moyen, J.-F. (2014). The processes that control leucosome compositions in metasedimentary granulites: perspectives from the Southern Marginal Zone migmatites, Limpopo Belt, South Africa. Journal of Metamorphic Geology, 32(7), 713–742. doi:10.1111/jmg.12087

Tindle, A.G. & Webb, P.C., 1994. PROBE-AMPH a spreadsheet to classify microprobe-derived amphibole analyses. Computers and Geosciences, 20, 1201-1228.

Tohver, E., Cawood, P.A., Rossello, E.A., López de Luchi, M.G., Rapalini, A.E., Jourdan, F., 2008. New SHRIMP u–Pb and 40Ar/39Ar constraints on the crustal stabilization of southern South America, from the margin of the Rio de Plata (Sierra de Ventana) craton to northern Patagonia., in: EOS Abstracts, American Geophysical Union, Fall Meeting. pp. T23C–2052.

Uriz, N.J., Cingolani, C.A., Chemale, F., Macambira, M.B., Armstrong, R., 2011. Isotopic studies on detrital zircons of Silurian–Devonian siliciclastic sequences from Argentinean North Patagonia and Sierra de la Ventana regions: comparative provenance. Int. J. Earth Sci. 100, 571–589. https://doi.org/10.1007/s00531-010-0597-z

Vallés, J., 1978. Los yacimientos de plomo “María Teresa” y “Tres Marías”, ejemplos de metalogénesis mesozoica en el Macizo Norpatagónico, Provincia de Río Negro., in: Actas. Presented at the VIII Congreso Geológico Argentino, pp. 71–78.

Varela, R., Basei, M.A.S, Sato, A.M., Siga, Jr., O., Cingolani, C., Sato, K., 1998. Edades isotópicos Rb/Sr y U/Pb en rocas de Mina Gonzalito y Arroyo Salado, Macizo Norpatagónico Atlántico, Río Negro, Argentina. Congreso Latinoamericano de Geología, X, Buenos Aires, Actas 1:71-76.

Varela, R., González, P.D., Basei, M.A.S, Sato, K., Sato, A., Naipauer, M., García, V., 2009. Complejo Mina Gonzalito, Patagonia: Nuevas Edades isotópicas e implicancias tectono-estratigráficas. in: Boletim de Resumos Expandidos, Simposio 45 Anos de Geocronologia no Brasil, pp 322-324

Varela, R., González, P.D., Basei, M.A.S., Sato, K., Sato, A.M., Naipauer, M., García, V.A., González, S., Greco, G., 2011. Edad del Complejo Mina Gonzalito: revisión y nuevos datos. In: Leanza, H., et al. (Eds.), XVIII Congreso Geológico Argentino. Neuquén, e-files, pp. 127-128

White, R.W., Powell, R. & Clarke, G.L., 2002. The interpretation of reaction textures in Fe-rich metapelitic granulites of the Musgrave Block, central Australia: Constraints from mineral equilibria calculations in the system K2O-FeO-MgO-Al2O3-SiO2-H2O-TiO2-Fe2O3. Journal of Metamorphic Geology, 20, 41-55.

Winchester, J.A., Floyd, P.A., 1977. Geochemical discrimination of different magma series and their differentiation products using immobile elements. Chem. Geol. 20, 325–343. https://doi.org/10.1016/0009-2541(77)90057-2

Appendix A.

Supplementary material A

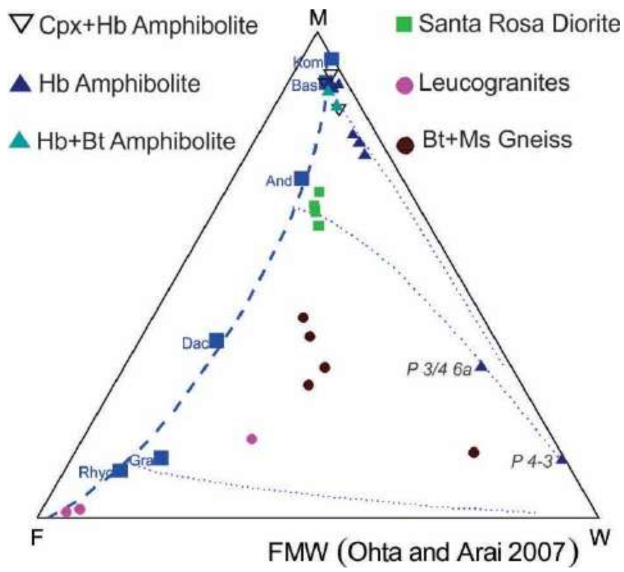

Supplementary material B

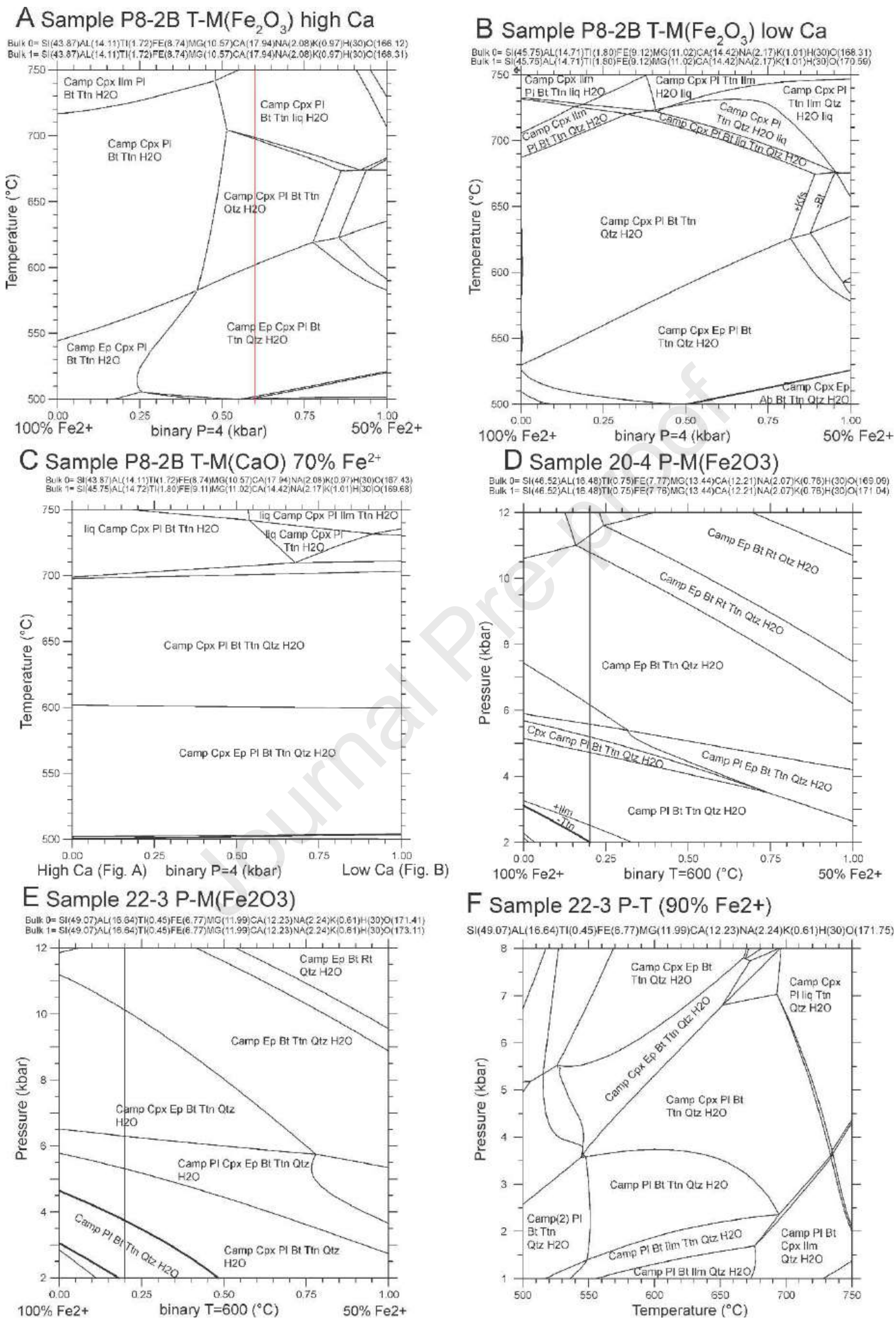
A Sample P8-2B T-M(Fe_2O_3) high Ca
B Sample P8-2B T-M(Fe_2O_3) low Ca
C Sample P8-2B T-M(CaO) 70% Fe^{2+}
D Sample 20-4 P-M(Fe2O3)
E Sample 22-3 P-M(Fe2O3)
F Sample 22-3 P-T (90% Fe2+)
Temperature (°C)
Pressure (kbar)
100% Fe2+
50% Fe2+
binary P=4 (kbar)
binary T=600 (°C)
High Ca (Fig. A)
Low Ca (Fig. B)
Camp Cpx Pl Bt Ttn Qtz H2O
Camp Cpx Ep Pl Bt Ttn Qtz H2O
Camp Ep Bt Ttn Qtz H2O
Camp Pl Bt Ttn Qtz H2O

957

Supplementary material C

	Mina Gonzalito	Subduction related- basalts*		Average MORB **			
		Island-Arc Tholeiites	High-Alumina and Calc-Alkaline Basalts	N-MORB	D-MORB	E-MORB	OIB ***
Ba/Zr	0.5-2	5	7.50	0.19	0.12	1.14	1.25
Ba/Nb	17- 49	157	214	5.41	4.75	7.35	7.29
Ba/Ce	3.4-13	30	13	1.58	1.14	4.92	4.38
La/Nb	0.5-2.7	1.86	7.14	1.16	1.30	0.70	0.77
Zr/Nb	14.2-31	31	29	28.15	38.58	6.45	5.83
Zr/Y	1.9-3.2	1.80	2.70	3.07	2.79	4.14	9.66
(Ce/Y)N[1]	0.63-1.7	1.20	3.50	0.22	0.17	0.55	6.38
Sm/Nd	0.2-0.3			0.32	0.35	0.25	0.26

*Sun (1980)

** Gale et al. (2013)

*** Sun and Mc Donough (1989)

[1] Normalized values to Chondrite of Thompson (1980), Ce = 0.865 and Y 2 ppm

Figure Captions

Figure 1. Location of the studied area in northern Patagonia and geological sketch of the Mina Gonzalito area and surroundings (modified from Martínez Dopico et al. 2011).

Figure 2. Geological sketch map of the Mina Gonzalito area showing the all the samples analized in this study. Based on Busteros et al. (1998) and González et al. (2008b).

Figure 3. View of the outcrops of Mina Gonzalito Complex. a) Contact between the amphibolites and the biotite schist; b) Detail of the texture in the biotite schists taken from outcrops to the west of Gonzalito mineschaft; c) Detail of the amphibolite exposures close to Puesto El Panchito.

Figure 4: Photomicrographs of the representative textures and features of the biotite bearing schists of the Mina Gonzalito Complex with plane (left) and crossed (right) polarized light. a) Texture of a schist located at Puesto Dragón (2 km to the south of Tres Marías mine). Note the red to yellow pleochroism of biotite; b) Texture of the schists close to El Panchito (?); c,d) Sample ASR-1 Porphyroblastic texture with larger crystals of plagioclase embedded in a lepidoblastic matrix of a gneiss of Estancia Santa Rosa.

Figure 5- a) Photomicrographs of the representative textures and features of the metamafic rocks of the Mina Gonzalito Complex a) amphibolite of north of Puesto El Panchito (P35) with plane (left) and crossed (right) polarizers showing nematoblastic texture; b) amphibolite of Gonzalito mine schaft (P9) with plane polarizers showing granoblastic blastic texture; c) Massive amphibolite taken from a section of a sequence of metamafic rocks in Polito mine schaft that grades into d) a banded amphibolite with lighter bands with plagioclase and diopside.

Figure 6. Photomicrographs of the samples used for the thermodynamic modelling with plane (left) and/or crossed (right) polarized light. a) Banded amphibolite from Tres Marías Mine (locality P31/32-3); b) Coarse-grained nematoblastic texture in an amphibolite from 1 km to the east of Mina Gonzalito mine camp (sample P20-4). Note the reddish-brown to yellow pleochroism of the hornblende crystals and the absence of quartz;

c) Granoblastic texture of metamafic rocks from north of Puesto El Panchito (P22), note the green to light green pleochroic hornblende.

Figure 7. Santa Rosa Diorite. Photomicrographs with plane (left) and crossed (right) polarized light of the representative textures and features of the diorites. Note the difference in the grain size. a) The fine-grained equigranular texture from sample ASR-2; b) Mafic clusters with green to dark green clinoamphibole plus yellow-brown biotite and opaque minerals; c) Worm texture in clinoamphibole and pyroxene cores -note the quartz exsolution after pyroxene-amphibole hydration reaction.

Figure 8. Geochemical classification of the sampled rocks of Mina Gonzalito Complex and Santa Rosa Diorite a) Total alkali versus SiO2 (Cox et al. 1979); b) AFM diagram of Miyashiro (1974); note the differential trend for the metamafic rocks; c) Zr/TiO2 versus Nb/Y plot of Winchester and Floyd (1977). Note the spread in the acidity of the rocks, the difference between the subtypes and the subalkaline tholeiitic affinity for the metamafic rocks.

Figure 9. Variation of selected major elements oxides (SiO2, Al2O3, CaO, K2O, P2O5, FeOt, Na2O) and Ni and V versus MgO (%). The grey diamonds correspond to the D-, N- and E-MORB compositions of Gale et al. (2013).

Figure 10. Chondrite normalized REE diagram for samples from the Mina Gonzalito Complex (metamafic rock with pyroxene –top left-, metamafic rocks with hornblende and/ or biotite –top right-, paragneisses and leucogranites –bottom left-) and Santa Rosa Diorite (bottom right). The normalizing chondrite REE values are from Boynton (1984). At the top, the D-MORB, N-MORB and E-MORB from Gale et al. (2013) are represented with dark grey, grey and light grey diamonds, respectively.

Figure 11. MORB normalized trace element diagrams for samples from the Mina Gonzalito Complex (metamafic rock with pyroxene –top left-, metamafic rocks with hornblende and/ or biotite –top right-, paragneisses and leucogranites –bottom left-) and Santa Rosa Diorite (bottom right). The normalizing MORB values are from Sun and McDonough (1989).

Figure 12. a) P-T pseudosection calculated based on the whole rock composition of samples a) ASR-1; b)31/32-3; b) P8-2b; c) d) 20-4; d)22-3. T where the interpreted peak field calculated with all iron as Fe2+ has bold outline and grey (light blue) colour infill. Camp is clinoamphibole, all other abbreviations from Kretz (1989); The interpreted peak field has bold outline. Camp is clinoamphibole, all other abbreviations from Kretz (1989).

Fig. 13. Venn diagram with the interpreted peak fields for all the samples.

Figure 14. Trace-elements-based tectonic environment discrimination plots a) The V-Ti/1000 diagram for metamafic rocks (Shervais, 1982); b) The Ti-Zr plot of Pearce (1982); and c) Nb-Zr-Y diagram applied for the distinction between mid-ocean ridge basalts and continental tholeiites from Meschede (1986).); c) La/10-Y/15-Nb/8 triangle of d) Th/Yb vs. Nb/Yb of Pearce et al. (2008) Note that the three independent parameters suggest that the metamafic rocks of Mina Gonzalito Complex have a volcanic arc to N-type MORBback-arc affinity. Symbols as in figure 8.

Figure 15. Geochronostratigraphic chart of the main Late Neoproterozoic to Paleozoic units and metamorphic and deformational events of the eastern North Patagonian Massif. Acronyms: TO Tardugno orthogneiss (Rapalini et al. 2013); PDP Playas Doradas pluton; SGP Sierra Grande pluton; ASP Arroyo Salado pluton (Pankhurst et al. 2006); EMP El Molino pluton (González et al. 2008a); PBP Peñas Blancas pluton (García et al. 2014); PNP Navarrete pluton; ATP Arroyo Tembrao pluton (Tohver et al. 2008); LVP La Verde pluton (García et al. 2012); SMP San Martín pluton (Pankhurst et al. 2006). Refences in text.

Table 1. Major and trace elements whole-rock geochemical analyses. The samples are located in the surrounding of Gonzalito Mine (MG), Tres Marías Mine (MTM), Puesto El Panchito (PEP), Polito mine shaft (P), Estancia Santa Rosa (ESR) and close to the Tapera Granite main outcrops close to Puesto Dragón (TAP); See figure 2 for reference location.

Sample	PG 6-Pique 11	P 8-2B	31/32-3	P 9-2A	P 4-3	20-3	20-4	35-2	GOP1-4	GOP1-3	15/16-1B	22-3	P 3/4 6a
Rock type	Banded metamafic rock	Banded metamafic rock	Banded metamafic rock	Hb (±Bt) metamafic rock	Hb (±Bt) metamafic rock	Hb (±Bt) metamafic rock	Hb (±Bt) metamafic rock	Hb (±Bt) metamafic rock	Hb metamafic rock *	Hb metamafic rock *	Hb metamafic rock	Hb metamafic rock	Hb metamafic rock *
Latitude (º) S	65 38 816	65 39 01	65 45 352	65 39 018	65 38 974	65 38 687	65 38 584	65 44 948	65 38 25	65 38 25	65 39 719	65 40 609	65 39 011
Longitude (º) W	41 19 212	41 19 04	41 18 411	41 19 125	42 18 943	41 18 897	41 18 907	41 18 368	41 19 00	41 19 00	41 20 362	41 19 042	41 18 909
SiO_2 (%)	45.28	45.74	48.4	48	48.04	47.41	49.14	50.78	50.13	51.07	48.48	52.16	56.17
TiO_2	2.87	2.39	0.82	1.3	1.11	2.14	1.05	0.61	1.45	1.37	1.47	0.64	1.71
Al_2O_3	14.28	12.48	15.42	13.78	12.99	14.26	14.77	14.63	13.6	15.15	16.09	15	14.3
Fe_2O_{3t}	12.62	12.11	10.34	14.83	19.17	17.42	10.9	8.44	12.25	11.62	12.86	9.56	13.55
MnO	0.26	0.17	0.26	0.34	2.59	0.23	0.17	0.15	0.17	0.16	0.19	0.17	0.22
MgO	5.81	7.39	7.14	7.65	4.92	6.88	9.52	9.46	6.92	6.55	6.38	8.55	5.15
CaO	14.56	17.46	15.31	9.2	0.54	10.17	12.04	12.19	8.01	8.69	12.02	12.13	1.87
Na_2O	1.15	1.12	1.43	0.64	0.09	1.3	1.13	1.1	0.62	0.83	1.25	1.23	0.46
K_2O	2.31	0.79	0.55	1.87	0.88	0.52	0.63	0.38	1.82	1.21	1.14	0.51	4.88
P_2O_5	0.43	0.41	0.07	0.19	0.1	0.19	0.08	0.06	0.11	0.15	0.11	0.06	0.21
LOI	1.26	0.79	0.83	2.2	*7.64*	0.32	1.31	1.11	5.44	4.07	0.91	0.96	2.26
SUM	100.83	100.85	100.57	100	98.07	100.84	100.74	98.91	100.52	100.87	100.9	100.97	100.78
Au	15	<5	<5	<5	25	11	35	10	21	<5	<5	<5	<5
As	3	<2	<2	10	76	<2	<2	<2	8	4	<2	<2	8
Br	<1	<1	<1	<1	<1	<1	<1	<1	<1	<1	<1	<1	<1
Co	49	60	47	50	25	71	52	48	41	40	57	50	42
Cr	270	328	81	164	141	114	69	279	270	310	276	132	95
Cs	3.5	2.3	0.5	7.1	2.6	2.2	4.8	1.8	5.7	4.5	2.3	2.5	12.6

Hf	3.9	2.9	1.6	1.8	1.8	2.8	1.6	0.5	2	2	2.1	1.4	4.8
Hg	<1	<1	<1	<1	<1	<1	<1	<1	<1	<1	<1	<1	<1
Ir	<5	<5	<5	<5	<5	<5	<5	<5	<5	<5	<5	<5	<5
Mo	<5	<5	<5	<5	<5	<5	<5	<5	<5	<5	<5	<5	<5
Rb	91	<20	<20	103	53	<20	<20	<20	140	75	46	<20	209
Sb	0.6	<0.2	<0.2	0.4	3.2	<0.2	<0.2	<0.2	0.4	<0.2	<0.2	<0.2	0.5
Sc	22.6	18.7	41	46.2	37.2	41.2	47.5	39.5	41	40	43	41.9	32.7
Se	<3	<3	<3	<3	<3	<3	5	<3	<3	<3	<3	<3	<3
Ta	3	2	1	<1	<1	2	<1	<1	<1	<1	<1	<1	<1
Th	2.3	2.9	2	0.6	1.2	<0.5	<0.5	<0.5	0.5	<0.5	<0.5	1	4.6
U	<0.5	1.2	<0.5	1.9	0.8	<0.5	<0.5	<0.5	0.7	0.8	0.9	<0.5	1.1
W	44	143	102	66	44	230	107	146	<3	<3	144	145	101
La	22.9	27.6	8.2	4.8	5.8	7.1	7.8	3.9	4.4	4.2	2.3	4.9	18.6
Ce	49	55	19	14	13	20	20	12	13	11	9	11	44
Nd	26	26	10	8	7	15	12	8	9	<5	7	6	25
Sm	5.3	4.9	2.6	2.7	2.3	4.3	3.1	1.6	2.4	2.4	2.7	1.8	5.4
Eu	1.8	1.5	0.9	1	0.6	1.4	0.8	0.5	1	1.1	1	0.6	0.7
Tb	0.7	0.6	0.6	<0.5	0.6	1.1	<0.5	<0.5	0.6	<0.5	<0.5	<0.5	1.2
Yb	1.4	1.3	2	3	2.2	4.3	2.6	1.6	2	2	3.2	1.7	4.8
Lu	0.22	0.18	0.3	0.42	0.3	0.58	0.36	0.25	0.28	0.28	0.47	0.22	0.71
Cu	48	34	110	518	383	80	99	51	56	67	37	69	114
Pb	137	50	9	1231	2957	16	49	6	<5	8	12	6	30
Zn	300	204	82	4327	10888	132	109	68	114	110	100	62	175
Ag	<0.4	<0.4	<0.4	1	1	<0.4	<0.4	0.7	0.6	<0.4	<0.4	<0.4	<0.4
Ni	142	244	76	88	104	100	102	114	76	73	101	86	53
Cd	1.5	2.6	<0.5	0.8	<0.5	0.7	0.9	0.5	0.7	0.7	<0.5	<0.5	0.5
Bi	<5	8	<5	<5	<5	<5	<5	<5	<5	<5	<5	<5	6
Ba	337	186	181	188	72	93	115	22	190	178	64	74	420
Sr	590	447	221	126	55	165	143	114	98	175	103	109	45
Y	26	20	24	31	22	43	28	16	21	22	33	18	48

Zr	172	153	61	59	58	100	89	41	84	82	63	39	179
Be	3	3	2	2	3	2	<1	<1	2	2	<1	<1	3
V	264	240	251	424	423	491	319	215	329	323	344	236	329
Nb	45	34	3	4	3	7	4	3	n.d.	n.d.	<2	2	11
S	110	240	<50	300	70	<50	<50	<50	n.d.	n.d.	<50	<50	1845
Ga	17	14	13	20	30	15	12	10	n.d.	n.d.	15	10	20
Sn	<5	<5	<5	<5	<5	<5	<5	<5	n.d.	n.d.	<5	<5	<5

Sample	ASR-6	ASR-2	ASR-3	ASR-5	ASR-4	15-1	ASR-1	GOP1-2	21-5	P 6-3	ASR-7	15/16-2	15/16-3B
Rock type	Diorite	Diorite	Diorite	Diorite	Diorite	Bt schist	Bt-Ms gneiss	Bt-schist	Bt schist	Ms+ Sill Leucogranite	Granite	Leucogranite	Leucogranite
Latitude (º) S	70 39 57	66 39 57	67 39 57	69 39 57	68 39 57	65 39 767	65 39 57	65 38 25	65 40 728	65 38 995	71 39 57	65 39 719	65 39 719
Longitude (º) W	46 23 03	42 23 03	43 23 03	45 23 03	44 23 03	41 20 310	41 23 03	41 19 00	41 17 764	41 19 035	47 23 03	41 20 362	41 20 362
SiO2 (%)	57.84	58.98	59.08	59.47	59.72	68.45	69.14	69.68	69.93	73.75	74.55	75.9	76.94
TiO2	1.13	1.1	1.13	1.13	1.13	0.7	0.69	0.7	0.74	0.02	0.41	0.08	0.02
Al2O3	14.81	14.82	15.06	14.94	15.02	14.34	14.21	13.4	13.35	14.85	12.83	13.63	13.79
Fe2O3	8.51	7.98	8.21	8.18	7.86	5.77	5.19	5.87	5.07	1.42	3.4	0.86	1.43
MnO	0.13	0.12	0.12	0.12	0.11	0.09	0.06	0.12	0.27	0.09	0.02	0.02	0.02
MgO	4.91	4.35	4.43	4.42	4.48	2.51	1.89	2.08	2.2	0.48	1.13	0.41	0.55
CaO	5.63	5.58	5.8	5.62	4.57	1.83	1.39	1.58	2.31	1.06	1.18	0.67	0.17
Na2O	2.69	2.5	2.68	2.57	2.67	2.63	2.44	2.05	2.37	2.14	2.08	2.82	1.6
K2O	2.45	2.94	2.83	2.93	3	2.74	3.57	3.49	2.32	5.06	3.86	5.09	4.43
P2O5	0.4	0.34	0.36	0.34	0.34	0.06	0.1	0.07	0.07	0.13	0.1	0.06	0.02

LOI	1.2	1	0.9	1.02	1.86	1.81	1.11	1.61	2.26	1.34	1.04	1.01	1.99
SUM	99.7	99.71	100.6	100.74	100.76	100.93	99.79	100.65	100.89	100.34	100.6	100.55	100.96
Au	10	18	5	12	14	5	7	14	5	5	5	5	13
As	<2	<2	<2	<2	<2	8	<2	8	<2	3	3	2	11
Br	<1	<1	<1	<1	<1	<1	<1	<1	<1	<1	<1	<1	<1
Co	25	23	23	21	23	25	11	14	30	16	9	29	32
Cr	270	230	210	180	210	54	230	220	54	6	310	6	7
Cs	4.1	3.7	3	3.1	3.4	4	2.3	4	3	2.2	3.8	3.4	3.2
Hf	5.5	6.8	5.7	5.2	6.4	6.6	6.4	7.6	14.4	1.6	5	1.4	1.4
Hg	<1	<1	<1	<1	<1	<1	<1	<1	<1	<1	<1	<1	<1
Ir	<5	<5	<5	<5	<5	<5	<5	<5	<5	<5	<5	<5	<5
Mo	<5	<5	<5	<5	<5	<5	<5	<5	<5	<5	<5	<5	<5
Rb	88	102	93	90	98	122	155	129	138	97	87	129	166
Sb	0.2	0.2	0.2	0.2	0.2	0.4	0.2	0.2	0.7	0.2	0.2	0.2	1.2
Sc	24	22	22	20	20	13.4	11	17	9.1	5.6	7	2.7	1.3
Se	<3	<3	<3	<3	<3	<3	<3	<3	<3	<3	<3	<3	<3
Ta	2	2	2	<1	<1	<1	3	1	2	<1	<1	2	1
Th	9.2	11	8.8	11	11	14.4	13	14	21.7	3	15	7.5	<0.5
U	<0.5	1.9	1.6	1.7	1.8	1.9	2.9	2.2	2.4	1.4	1.8	1.9	0.5
W	<3	<4	<5	<6	<7	167	3	3	251	196	3	376	369
La	36.3	40.5	38	34.6	26.9	44.5	39.4	39.5	60.4	11.5	38.6	18.6	2.3
Ce	75	80	76	66	60	89	81	81	122	22	72	36	3
Nd	33	35	40	31	30	36	40	36	56	10	35	15	<5
Sm	7.3	7.5	7.2	6.4	6.3	6.4	7.4	7	10.2	1.8	7.6	2.5	0.3
Eu	1.8	1.9	1.8	1.6	1.6	1.3	1.5	1.7	1.7	1.7	1.4	0.6	0.4
Tb	0.5	1.3	1	0.9	1.2	1.1	1.3	1.4	1.9	<0.5	<0.5	<0.5	<0.5
Yb	2.7	2.6	2.9	2.6	2.5	2.8	2.8	4.3	1.1	3.1	1.4	1.4	0.4
Lu	0.39	0.39	0.41	0.34	0.36	0.41	0.41	0.67	0.17	0.45	0.23	0.22	0.06

Cu	30	8	28	10	87	13	11	19	7	8	23	11	19
Pb	12	11	18	9	11	46	24	90	100	103	34	67	124
Zn	111	107	104	111	100	117	89	343	144	117	58	102	369
Ag	<0.4	<0.4	<0.4	<0.4	<0.4	0.6	<0.4	<0.4	3.8	<0.4	<0.4	<0.4	<0.4
Ni	32	31	30	31	29	28	22	30	35	7	19	16	17
Cd	<0.5	<0.5	<0.5	<0.5	<0.5	<0.5	<0.5	0.7	<0.5	0.7	<0.5	<0.5	<0.5
Bi	<5	<5	<5	<5	<5	<5	<5	<5	<5	<5	<5	<5	<5
Ba	771	892	888	885	901	381	631	673	500	1261	938	842	635
Sr	465	491	496	492	473	316	177	163	226	225	197	248	64
Y	32	31	32	31	30	44	47	35	22	22	24	14	2
Zr	211	237	230	236	251	306	265	320	697	43	168	35	4
Be	2	3	3	3	3	3	2	<1	2	3	<1	2	2
V	192	203	212	199	199	121	77	86	85	<5	50	15	37
Nb	n.d.	n.d.	n.d.	n.d.	n.d.	18	n.d.	n.d.	14	<2	n.d.	6	<2
S	n.d.	n.d.	n.d.	n.d.	n.d.	75	n.d.	n.d.	<50	<50	n.d.	<50	<50
Ga	n.d.	n.d.	n.d.	n.d.	n.d.	18	n.d.	n.d.	14	11	n.d.	13	15
Sn	n.d.	n.d.	n.d.	n.d.	n.d.	<5	n.d.	n.d.	<5	<5	n.d.	<5	<5

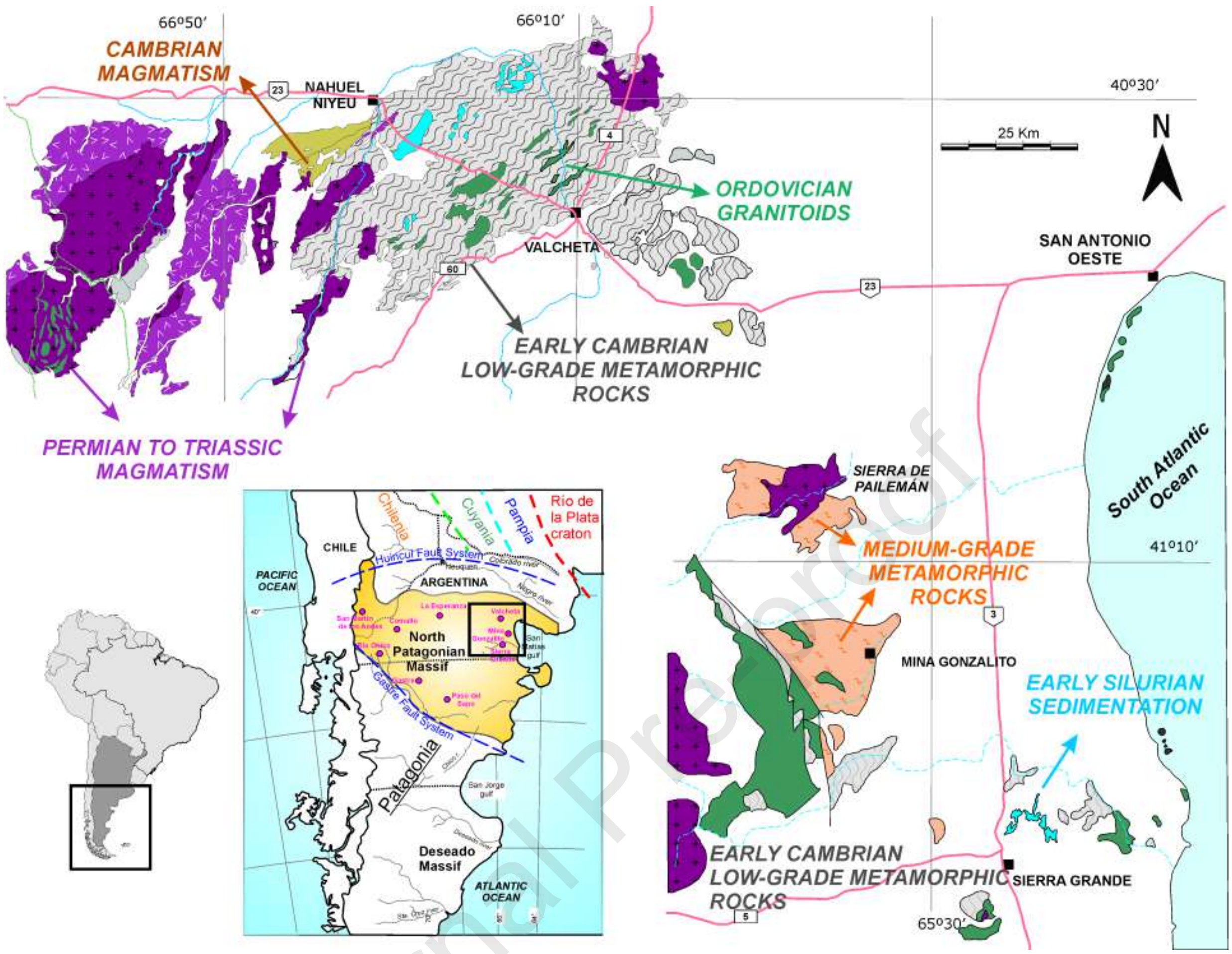

66º50′
66º10′
40º30′
41º10′
65º30′
CAMBRIAN MAGMATISM
NAHUEL NIYEU
VALCHETA
ORDOVICIAN GRANITOIDS
SAN ANTONIO OESTE
EARLY CAMBRIAN LOW-GRADE METAMORPHIC ROCKS
PERMIAN TO TRIASSIC MAGMATISM
25 Km
N
SIERRA DE PAILEMÁN
South Atlantic Ocean
MEDIUM-GRADE METAMORPHIC ROCKS
MINA GONZALITO
EARLY SILURIAN SEDIMENTATION
SIERRA GRANDE
Chilenia
Cuyania
Pampia
Rio de la Plata craton
CHILE
ARGENTINA
PACIFIC OCEAN
Huincul Fault System
North Patagonian Massif
Gastre Fault System
Patagonia
Deseado Massif
ATLANTIC OCEAN
San Jorge gulf

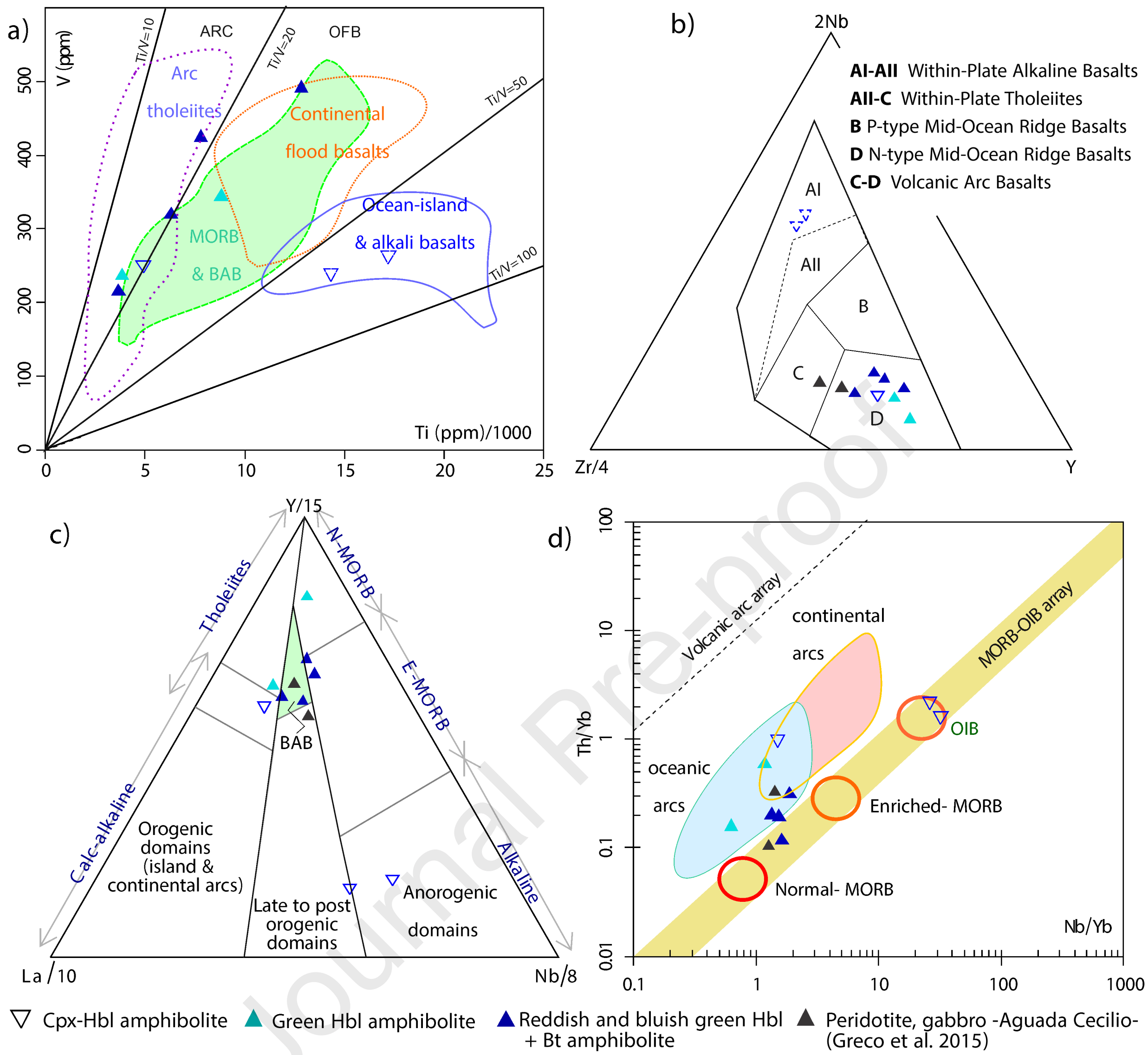

a)
V (ppm)
Ti (ppm)/1000
ARC
OFB
Ti/V=10
Ti/V=20
Ti/V=50
Ti/V=100
Arc
tholeiites
Continental
flood basalts
MORB
& BAB
Ocean-island
& alkali basalts
b)
2Nb
Zr/4
Y
AI-AII Within-Plate Alkaline Basalts
AII-C Within-Plate Tholeiites
B P-type Mid-Ocean Ridge Basalts
D N-type Mid-Ocean Ridge Basalts
C-D Volcanic Arc Basalts
AI
AII
B
C
D
c)
Y/15
La/10
Nb/8
Tholeiites
Calc-alkaline
N-MORB
E-MORB
Alkaline
BAB
Orogenic domains (island & continental arcs)
Late to post orogenic domains
Anorogenic domains
d)
Th/Yb
Nb/Yb
Volcanic arc array
MORB-OIB array
continental arcs
oceanic arcs
OIB
Enriched- MORB
Normal- MORB
Cpx-Hbl amphibolite
Green Hbl amphibolite
Reddish and bluish green Hbl + Bt amphibolite
Peridotite, gabbro -Aguada Cecilio- (Greco et al. 2015)

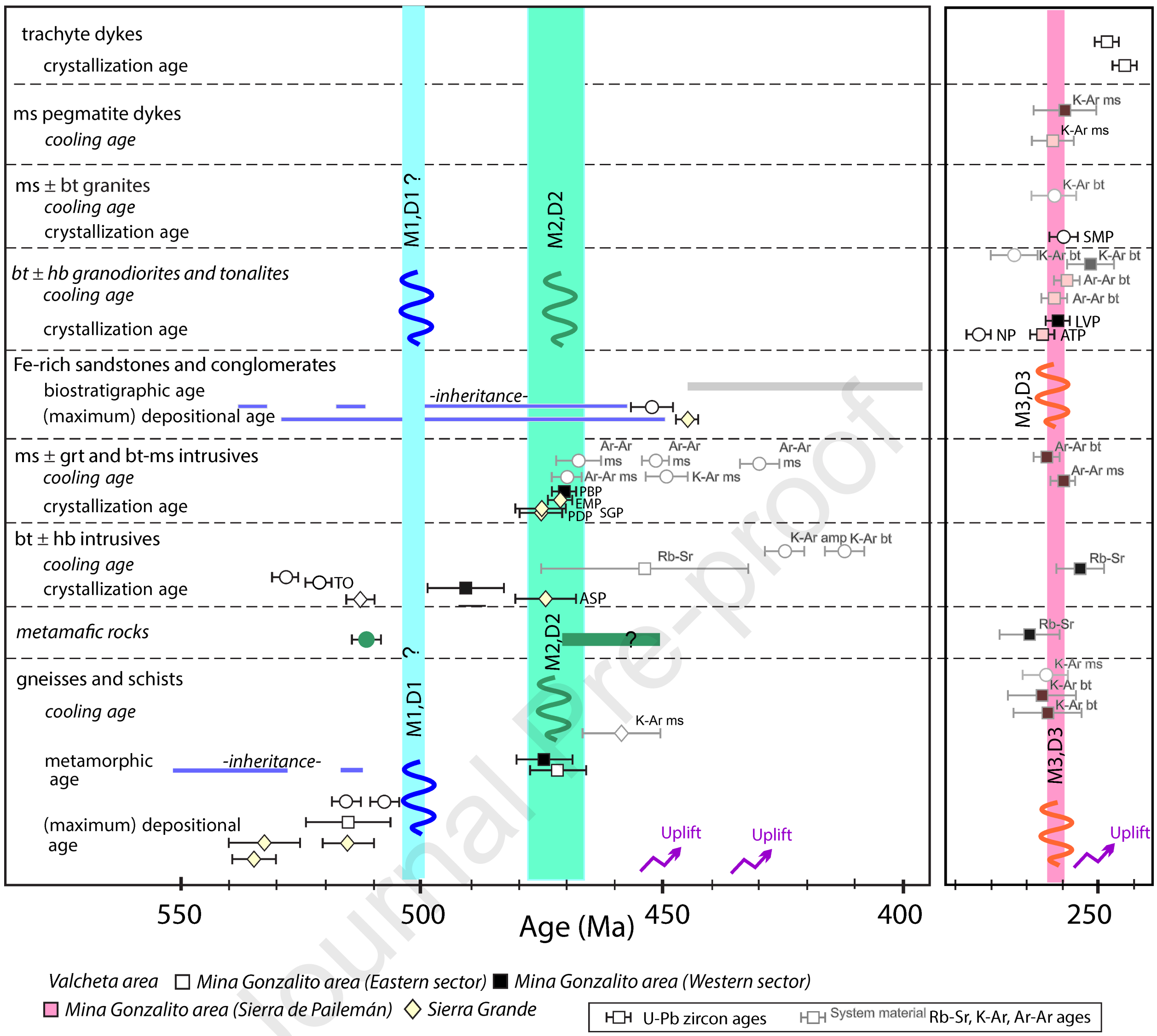

trachyte dykes
crystallization age
ms pegmatite dykes
cooling age
ms ± bt granites
cooling age
crystallization age
bt ± hb granodiorites and tonalites
cooling age
crystallization age
Fe-rich sandstones and conglomerates
biostratigraphic age
(maximum) depositional age
-inheritance-
ms ± grt and bt-ms intrusives
cooling age
crystallization age
bt ± hb intrusives
cooling age
crystallization age
metamafic rocks
gneisses and schists
cooling age
metamorphic age
-inheritance-
(maximum) depositional age
M1,D1 ?
M1,D1
M2,D2
M3,D3
Uplift
Age (Ma)
550
500
450
400
250
Valcheta area
Mina Gonzalito area (Eastern sector)
Mina Gonzalito area (Western sector)
Mina Gonzalito area (Sierra de Pailemán)
Sierra Grande
U-Pb zircon ages
System material Rb-Sr, K-Ar, Ar-Ar ages

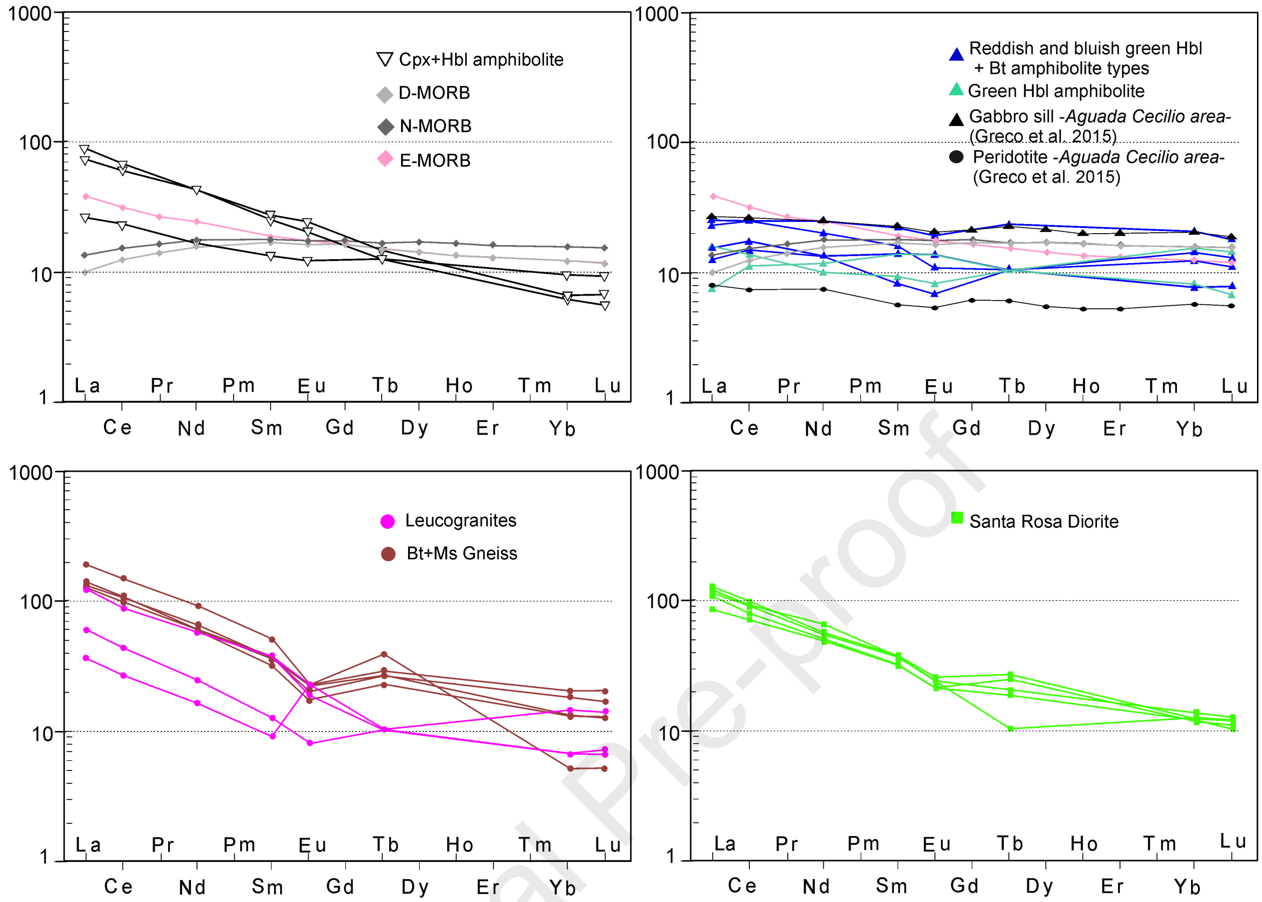
Cpx+Hbl amphibolite
D-MORB
N-MORB
E-MORB
Reddish and bluish green Hbl + Bt amphibolite types
Green Hbl amphibolite
Gabbro sill -Aguada Cecilio area- (Greco et al. 2015)
Peridotite -Aguada Cecilio area- (Greco et al. 2015)
Leucogranites
Bt+Ms Gneiss
Santa Rosa Diorite
1000
100
10
1
La Pr Pm Eu Tb Ho Tm Lu
Ce Nd Sm Gd Dy Er Yb

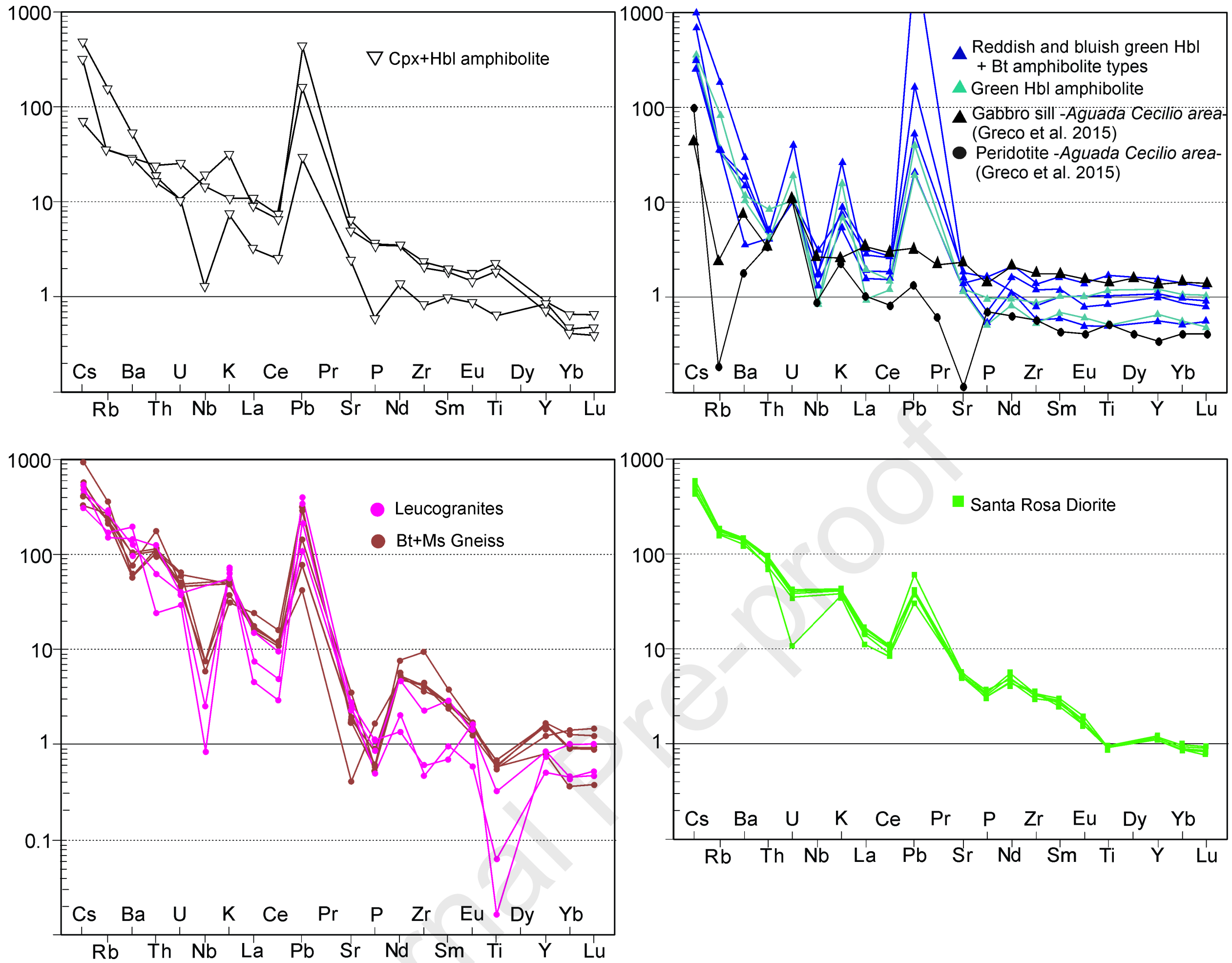

Cpx+Hbl amphibolite
Reddish and bluish green Hbl + Bt amphibolite types
Green Hbl amphibolite
Gabbro sill -Aguada Cecilio area- (Greco et al. 2015)
Peridotite -Aguada Cecilio area- (Greco et al. 2015)
Leucogranites
Bt+Ms Gneiss
Santa Rosa Diorite
1000
100
10
1
0.1
Cs Ba U K Ce Pr P Zr Eu Dy Yb
Rb Th Nb La Pb Sr Nd Sm Ti Y Lu

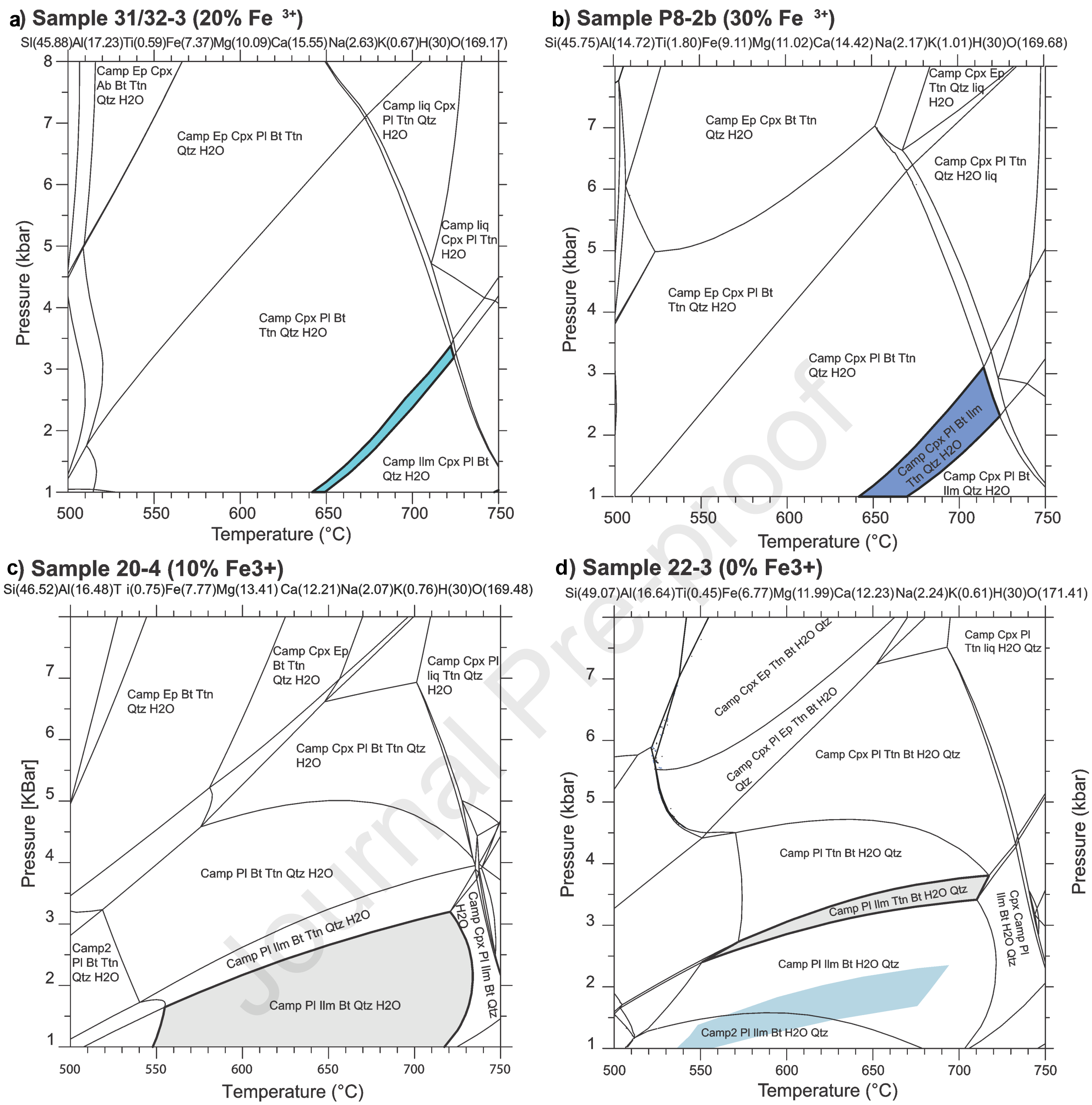
a) Sample 31/32-3 (20% Fe 3+)
SI(45.88)Al(17.23)Ti(0.59)Fe(7.37)Mg(10.09)Ca(15.55)Na(2.63)K(0.67)H(30)O(169.17)
Camp Ep Cpx Ab Bt Ttn Qtz H2O
Camp Ep Cpx Pl Bt Ttn Qtz H2O
Camp liq Cpx Pl Ttn Qtz H2O
Camp liq Cpx Pl Ttn H2O
Camp Cpx Pl Bt Ttn Qtz H2O
Camp Ilm Cpx Pl Bt Qtz H2O
Pressure (kbar)
Temperature (°C)
b) Sample P8-2b (30% Fe 3+)
Si(45.75)Al(14.72)Ti(1.80)Fe(9.11)Mg(11.02)Ca(14.42)Na(2.17)K(1.01)H(30)O(169.68)
Camp Cpx Ep Ttn Qtz liq H2O
Camp Ep Cpx Bt Ttn Qtz H2O
Camp Cpx Pl Ttn Qtz H2O liq
Camp Ep Cpx Pl Bt Ttn Qtz H2O
Camp Cpx Pl Bt Ttn Qtz H2O
Camp Cpx Pl Bt Ilm Ttn Qtz H2O
Camp Cpx Pl Bt Ilm Qtz H2O
Pressure (kbar)
Temperature (°C)
c) Sample 20-4 (10% Fe3+)
Si(46.52)Al(16.48)T i(0.75)Fe(7.77)Mg(13.41) Ca(12.21)Na(2.07)K(0.76)H(30)O(169.48)
Camp Ep Bt Ttn Qtz H2O
Camp Cpx Ep Bt Ttn Qtz H2O
Camp Cpx Pl liq Ttn Qtz H2O
Camp Cpx Pl Bt Ttn Qtz H2O
Camp Pl Bt Ttn Qtz H2O
Camp2 Pl Bt Ttn Qtz H2O
Camp Pl Ilm Bt Ttn Qtz H2O
Camp Pl Ilm Bt Qtz H2O
Camp Cpx Pl Ilm Bt Qtz H2O
Pressure [KBar]
Temperature (°C)
d) Sample 22-3 (0% Fe3+)
Si(49.07)Al(16.64)Ti(0.45)Fe(6.77)Mg(11.99)Ca(12.23)Na(2.24)K(0.61)H(30)O(171.41)
Camp Cpx Pl Ttn liq H2O Qtz
Camp Cpx Ep Ttn Bt H2O Qtz
Camp Cpx Pl Ep Ttn Bt H2O Qtz
Camp Cpx Pl Ttn Bt H2O Qtz
Camp Pl Ttn Bt H2O Qtz
Camp Pl Ilm Ttn Bt H2O Qtz
Camp Pl Ilm Bt H2O Qtz
Camp2 Pl Ilm Bt H2O Qtz
Cpx Camp Pl Ilm Bt H2O Qtz
Pressure (kbar)
Temperature (°C)

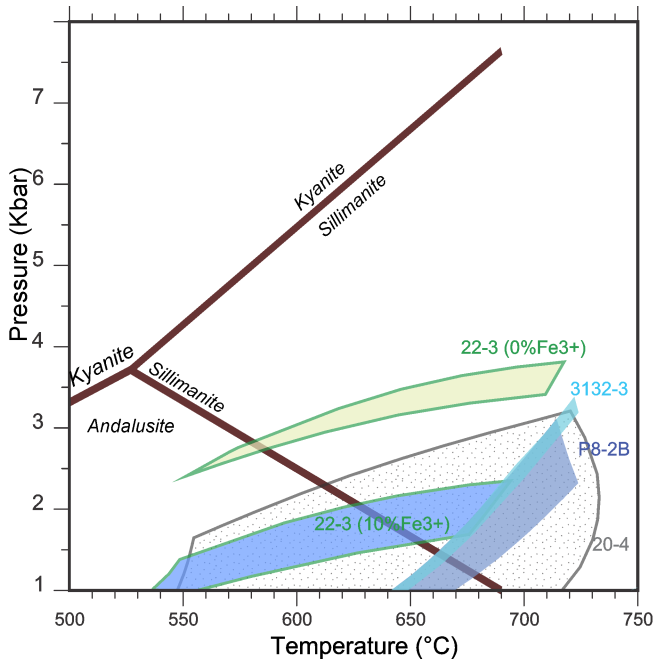

Pressure (Kbar)
Temperature (°C)
Kyanite
Sillimanite
Andalusite
22-3 (0%Fe3+)
3132-3
P8-2B
22-3 (10%Fe3+)
20-4

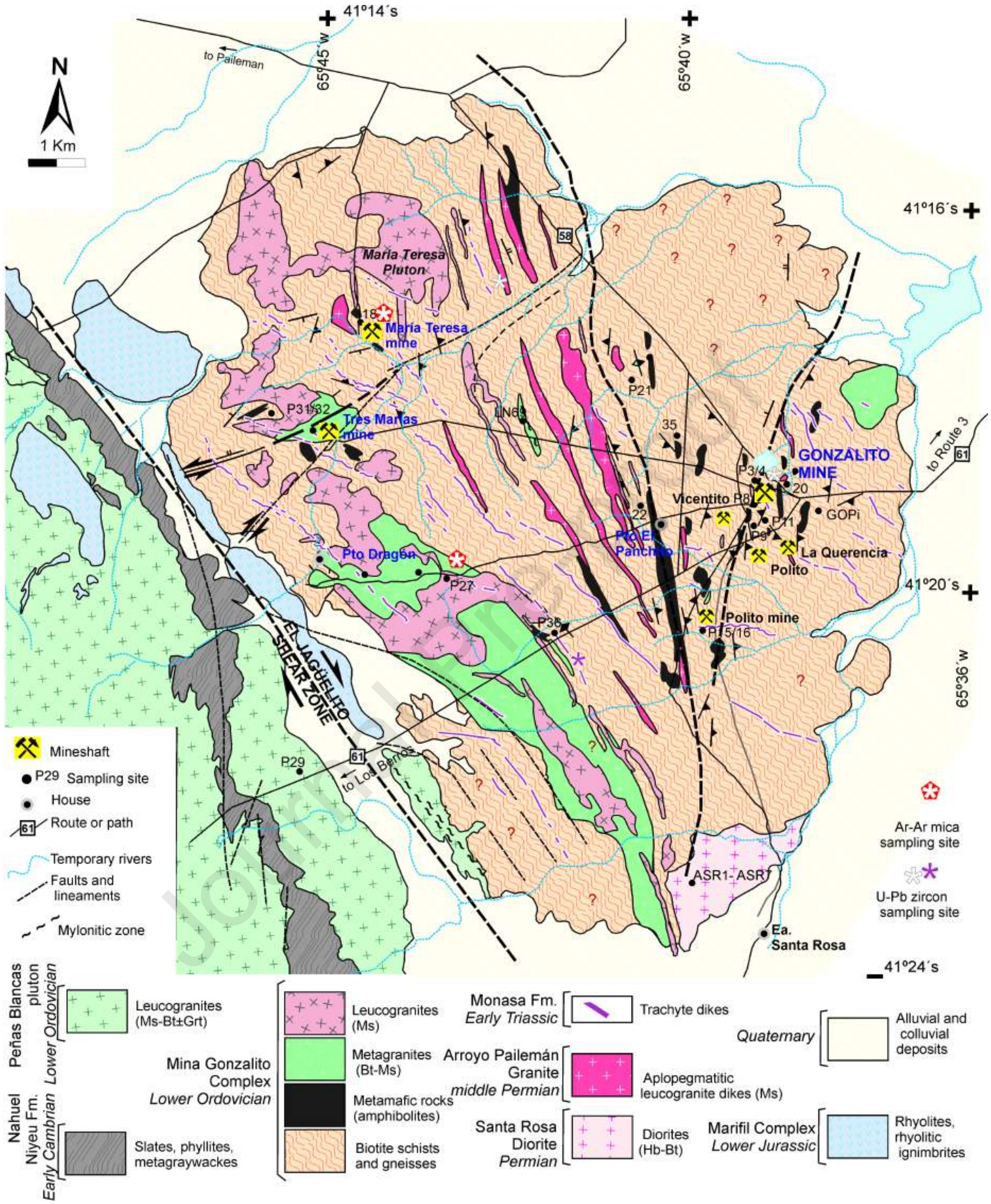

41º14´s
65º45´w
65º40´w
41º16´s
41º20´s
65º36´w
41º24´s
N
1 Km
to Paileman
María Teresa Pluton
María Teresa mine
Tres Marías mine
GONZALITO MINE
Vicentito
La Querencia
Polito
Polito mine
Pto Dragón
Pto El Panchito
EL JAGÜELITO SHEAR ZONE
to Los Berros
to Route 3
Ea. Santa Rosa
Mineshaft
P29 Sampling site
House
Route or path
Temporary rivers
Faults and lineaments
Mylonitic zone
Ar-Ar mica sampling site
U-Pb zircon sampling site
Peñas Blancas pluton Lower Ordovician
Leucogranites (Ms-Bt±Grt)
Nahuel Niyeu Fm. Early Cambrian
Slates, phyllites, metagraywackes
Mina Gonzalito Complex Lower Ordovician
Leucogranites (Ms)
Metagranites (Bt-Ms)
Metamafic rocks (amphibolites)
Biotite schists and gneisses
Monasa Fm. Early Triassic
Trachyte dikes
Arroyo Pailemán Granite middle Permian
Aplopegmatitic leucogranite dikes (Ms)
Santa Rosa Diorite Permian
Diorites (Hb-Bt)
Quaternary
Alluvial and colluvial deposits
Marifil Complex Lower Jurassic
Rhyolites, rhyolitic ignimbrites

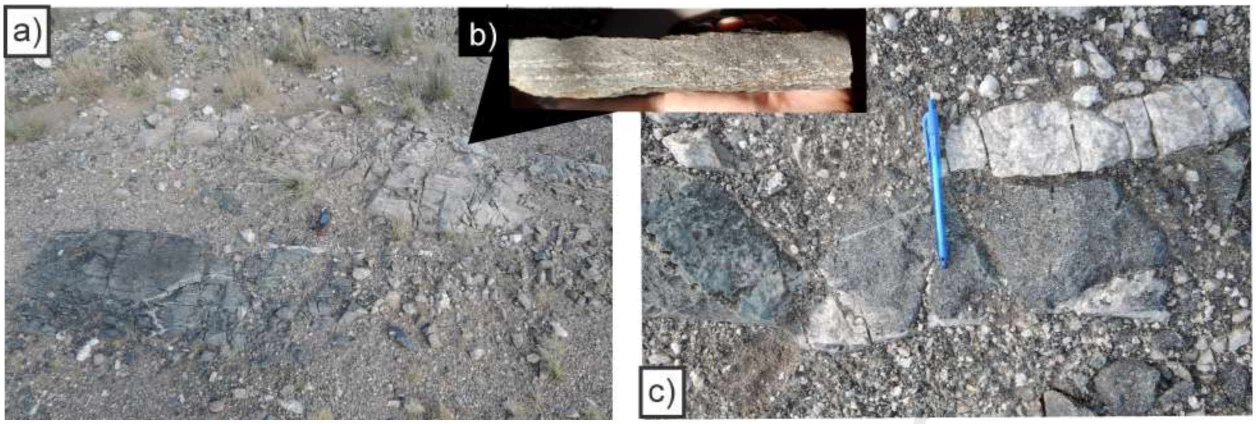
a)
b)
c)

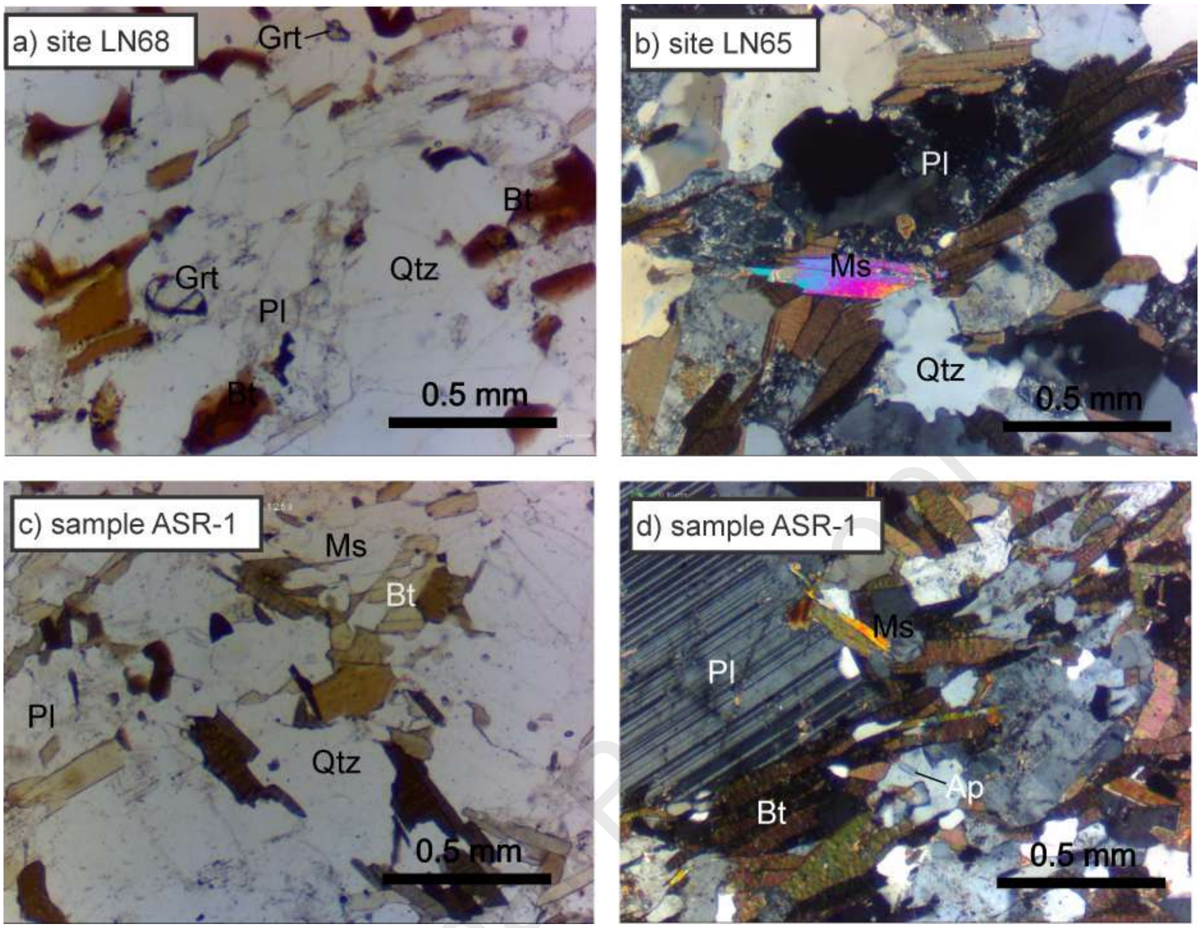
a) site LN68
Grt
Bt
Grt
Pl
Qtz
Bt
0.5 mm
b) site LN65
Pl
Ms
Qtz
0.5 mm
c) sample ASR-1
Ms
Bt
Pl
Qtz
0.5 mm
d) sample ASR-1
Ms
Pl
Ap
Bt
0.5 mm

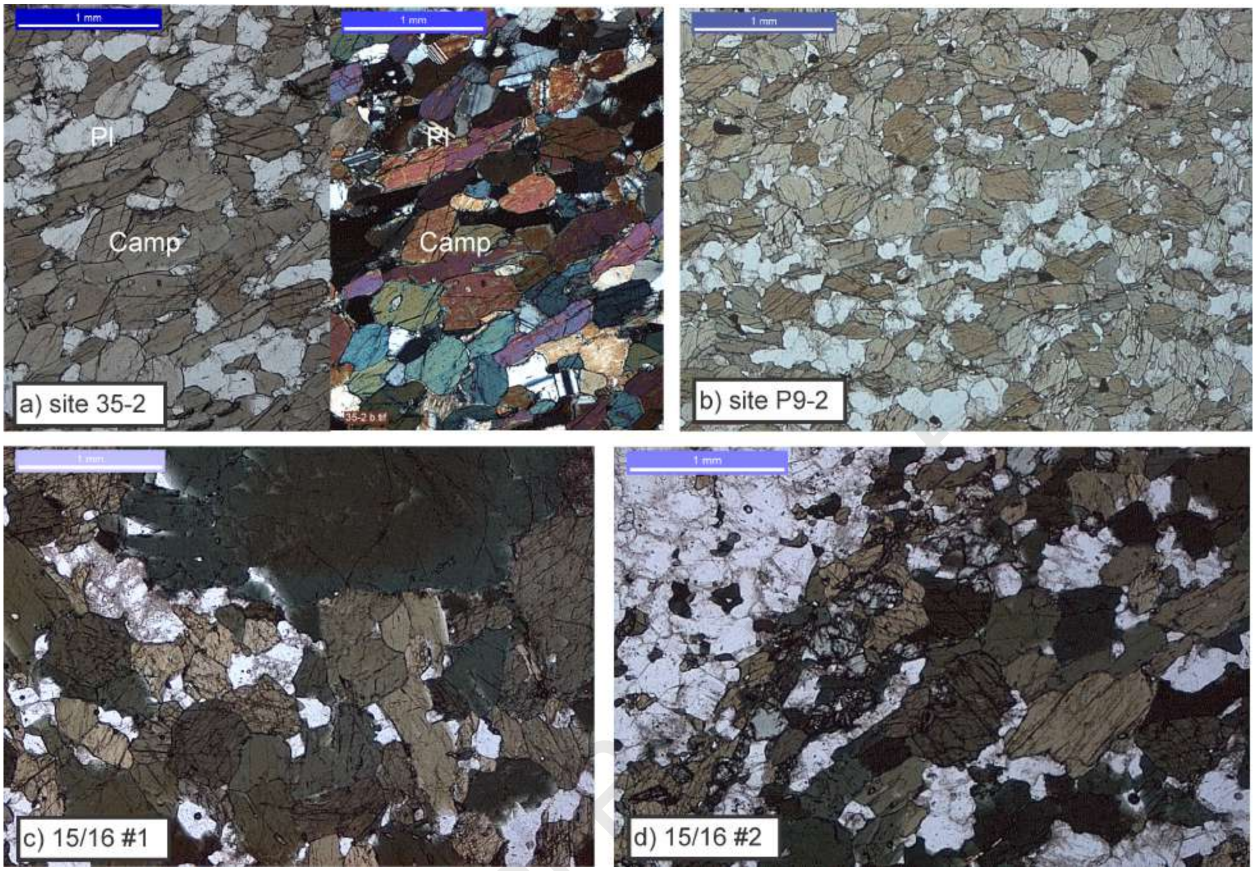
1 mm
1 mm
Pl
Pl
Camp
Camp
a) site 35-2
1 mm
b) site P9-2
1 mm
c) 15/16 #1
1 mm
d) 15/16 #2

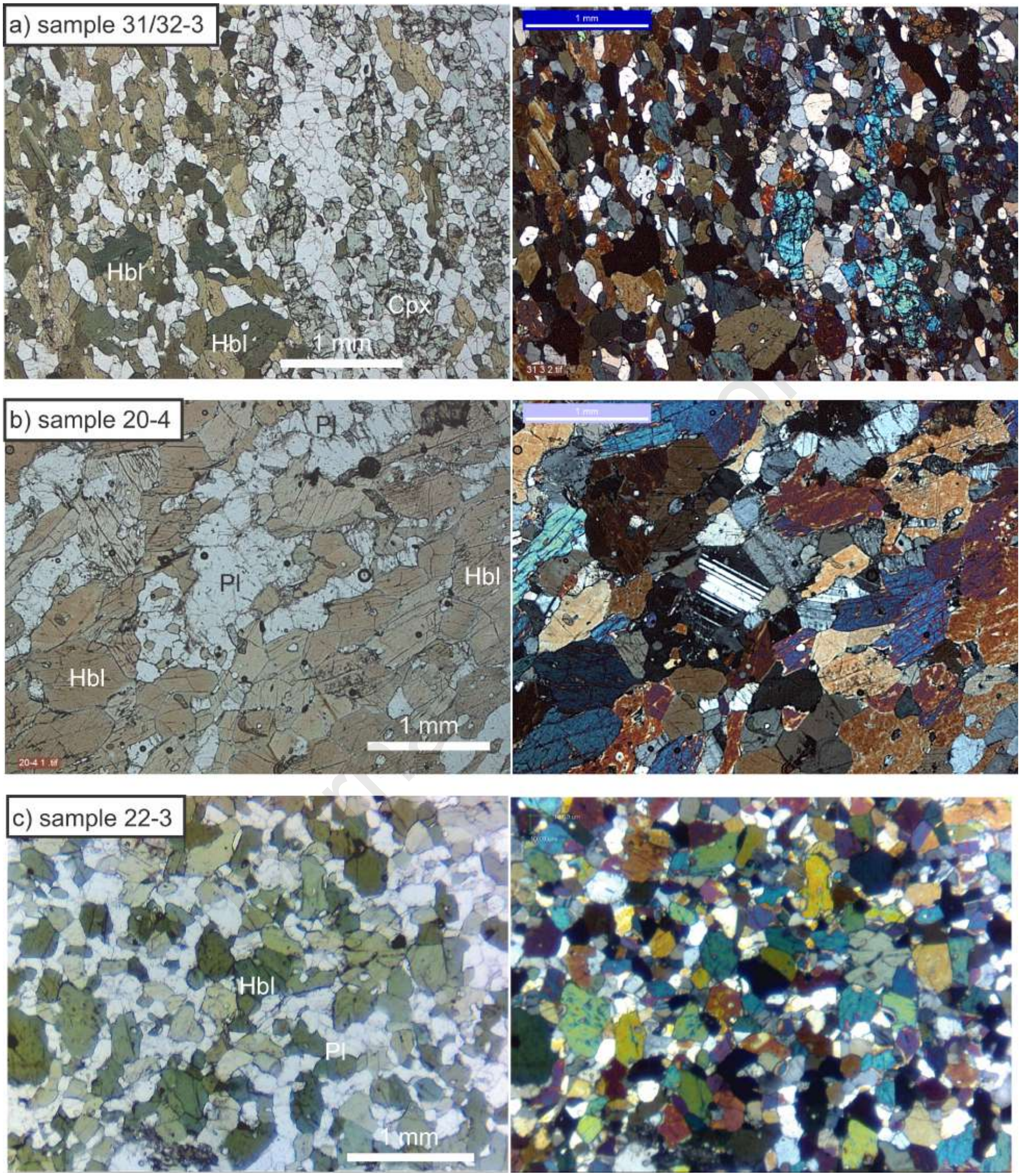
a) sample 31/32-3
Hbl
Hbl
Cpx
1 mm
1 mm
b) sample 20-4
Pl
Pl
Hbl
Hbl
1 mm
1 mm
c) sample 22-3
Hbl
Pl
1 mm

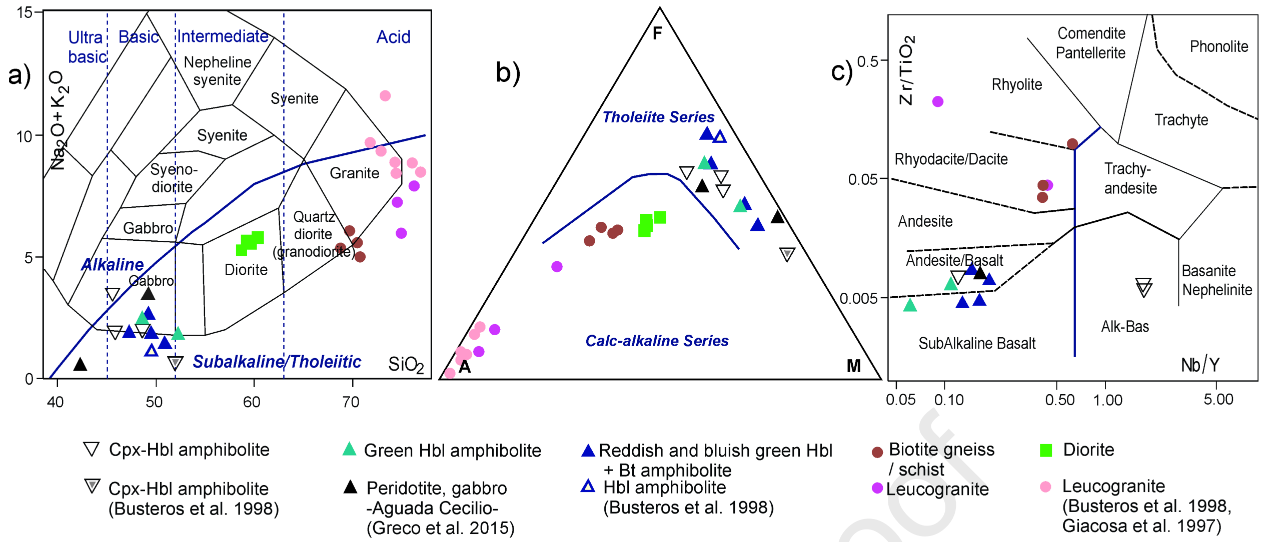
a)
Na2O+K2O
Ultra basic
Basic
Intermediate
Acid
Nepheline syenite
Syenite
Syenite
Syeno-diorite
Granite
Gabbro
Quartz diorite (granodiorite)
Alkaline
Gabbro
Diorite
Subalkaline/Tholeiitic
SiO2
b)
F
Tholeiite Series
Calc-alkaline Series
A
M
c)
Zr/TiO2
Comendite Pantellerite
Phonolite
Rhyolite
Trachyte
Rhyodacite/Dacite
Trachy-andesite
Andesite
Andesite/Basalt
Basanite Nephelinite
Alk-Bas
SubAlkaline Basalt
Nb/Y
Cpx-Hbl amphibolite
Cpx-Hbl amphibolite (Busteros et al. 1998)
Green Hbl amphibolite
Peridotite, gabbro -Aguada Cecilio- (Greco et al. 2015)
Reddish and bluish green Hbl + Bt amphibolite
Hbl amphibolite (Busteros et al. 1998)
Biotite gneiss / schist
Leucogranite
Diorite
Leucogranite (Busteros et al. 1998, Giacosa et al. 1997)

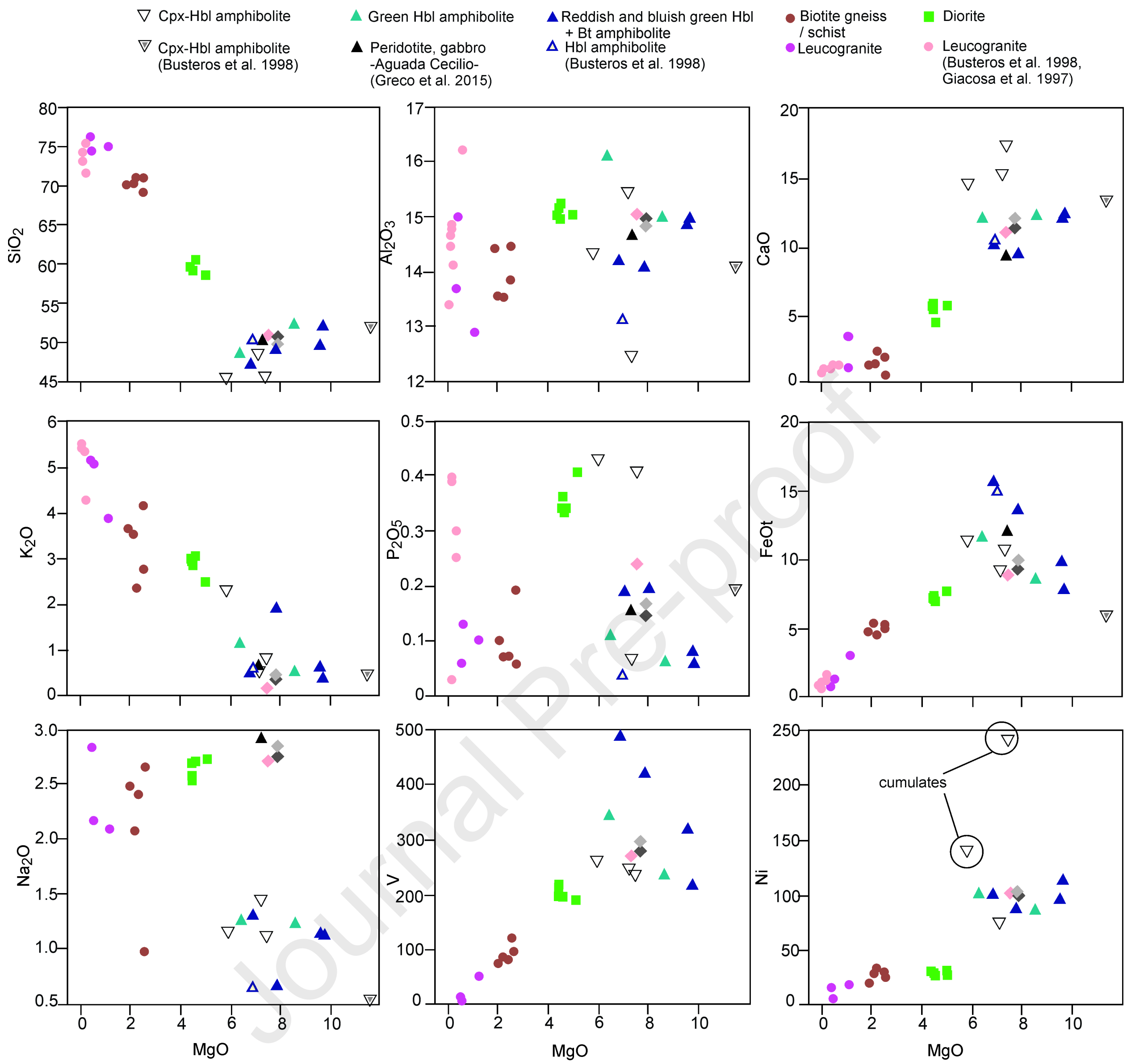

Cpx-Hbl amphibolite
Cpx-Hbl amphibolite (Busteros et al. 1998)
Green Hbl amphibolite
Peridotite, gabbro -Aguada Cecilio- (Greco et al. 2015)
Reddish and bluish green Hbl + Bt amphibolite
Hbl amphibolite (Busteros et al. 1998)
Biotite gneiss / schist
Leucogranite
Diorite
Leucogranite (Busteros et al. 1998, Giacosa et al. 1997)
SiO2
Al2O3
CaO
K2O
P2O5
FeOt
Na2O
V
Ni
cumulates
MgO
MgO
MgO

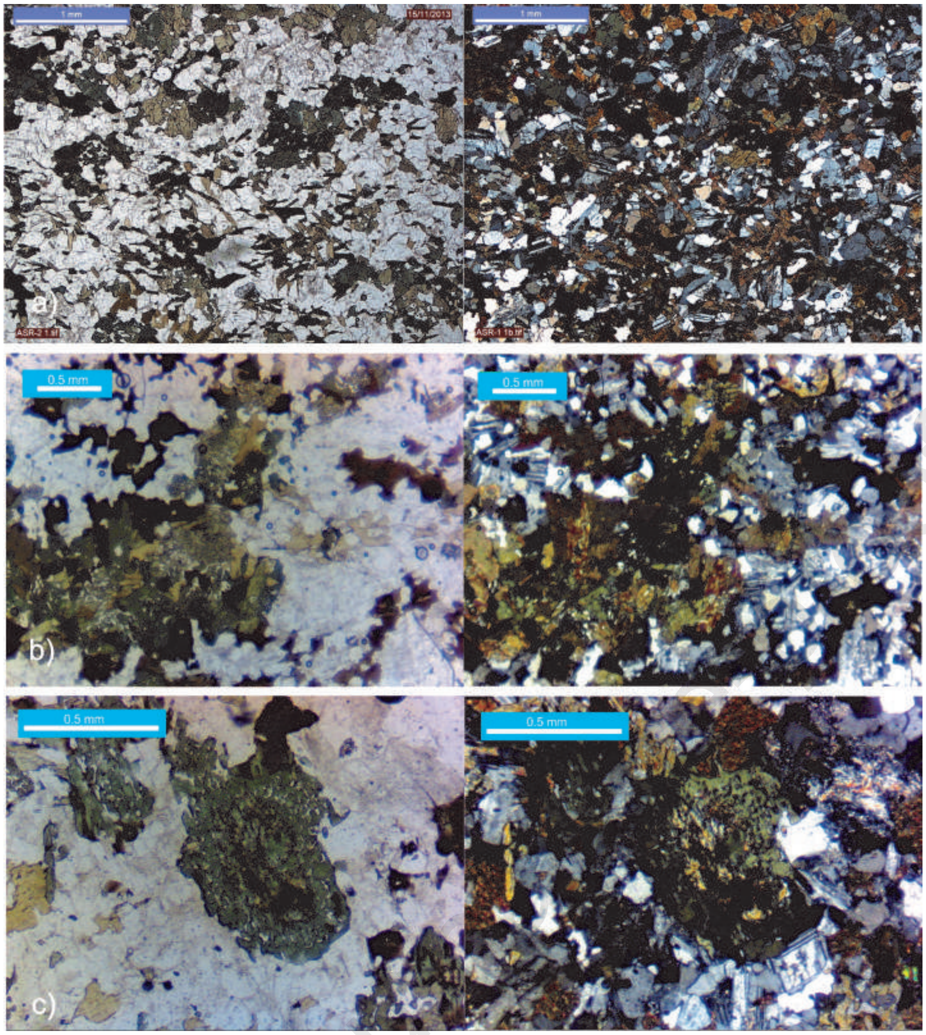
1 mm
15/11/2013
1 mm
a)
ASR-2 1.tif
ASR-1 1b.tif
0.5 mm
0.5 mm
b)
0.5 mm
0.5 mm
c)

Highlights

+ Mina Gonzalito Complex is reinterpreted as having a larger proportion of (mafic to intermediate) metaigneous protoliths than previously proposed

+ Massive, foliated and banded gabbros are the main protoliths of the metamafic rocks

+ Metamafic rocks were likely emplaced in a back-arc tectonic setting

Carmen I. Martínez Dopico: conceptualization; methodology; visualization; writing; funding acquisition; editing; review

Kathryn A. Cutts: conceptualization; visualization; writing, editing; review

Mónica G. López de Luchi: conceptualization; resources; validation; supervision; review

Franco Pugliese: conceptualization; validation; writing; review

Declaration of interests

☒ The authors declare that they have no known competing financial interests or personal relationships that could have appeared to influence the work reported in this paper.

☐The authors declare the following financial interests/personal relationships which may be considered as potential competing interests: